REVIEW

J. Indian Chem. Soc.,
Vol. 97, May 2020, pp. 693-719

Addressing analytical challenges in estimation of precious metals (Ag, Au, Pd, Pt) across a wide range of samples†

Manish Banerjee

Geo-Scientist, Chemical Division, Geological Survey of India, Northern Region, Aliganj, Lucknow-226 024, Uttar Pradesh, India

E-mail: manish.banerjee@gsi.gov.in

Manuscript received online 30 December 2019, revised and accepted 26 March 2020

With the rapid development of technology, new and improved materials have become indispensable in our daily life. Consequently, certain metals have gained immense importance compared to others as more and more mature materials are evolving. One such group is the precious metals comprising mainly silver, gold, palladium and platinum. Their application ranges from jewelry and kitchen wares to sensors, energy storage and conversion devices, electronic circuits, etc. Following this global realization most of the developed and developing countries have extended their effort to find and extract these elements from nature. This has led to several geochemical mapping programs in these countries to trace these elements. Moreover, applications of these metals have led to extensive use contributing to heavy metal footprints in the environment. The consequent accumulation of the elements in the natural environment causes detrimental effect on human beings and other living organisms. Therefore, sometimes it becomes necessary to enhance the analytical ability of the technique to trace the metals to ppb and sub-ppb level, for "chemical autopsy" of the samples to enhance ecological consciousness in the society. Analysis of samples of diverse origin such as archaeological, geological, environmental, waste materials, industrial, nanomaterials, biomaterials, etc. have been addressed. Spectroscopic techniques, with various internal modifications have played a crucial role in the determination of these elements. The present review comprises of the multiple spectroscopic and non-spectroscopic techniques, including destructive and non-destructive techniques, and their modification available in order to precisely determine the precious metals in samples of different backgrounds.

Keywords: Precious metals, spectroscopy, chemosensor, non-destructive, analysis.

1. Introduction

The application of precious metals especially silver, gold, palladium and platinum has come a long way from ornament and jewelry to various segments of modern application such as catalysis, sensors, imaging, photonics, biomaterials and electronics, among others, which is leading the future of new and improved materials. Their modern applications mainly dwell on their attractive optical, electrical, magnetic, and chemical properties[1–8]. Now, owing to these facts the precious metals play a pivotal role in the development of technology and therefore, the progress of economy. Consequently, there has been an increasing effort from developing and developed countries to extract these elements from nature which in turn has paved the way for geochemical mapping across the length and breadth of the country at suitably close intervals. Extensive use of these metals leads to their higher concentration in the environment and enhances health hazard. This gigantic analytical task requires techniques with high precision, robust instruments, high throughput, enhanced sensitivity, economical methods, and suitable digestion and extraction methods, in order to combat their low crustal abundance[9,10] and their intrinsic chemical inertness. Therefore, environmental monitoring for metal footprints becomes quintessential.

Silver has been generously used in water treatment, bone prostheses, orthopedic surgery, catheters, cardiac devices, healing, and surgical appliances. Although silver is known to have some antimicrobial property, accumulation of silver in the form of insoluble silver precipitates (silver metal or silver sulfide/selenide) in the skin (argyria), eye (argyrosis) and other organs due to clinical exposure can be very harmful[11,12]. Ag^+ is also known to replace essential ions in hydroxyapa-

†This review article is dedicated to late Shri Ashoke Chatterjee and late Professor Nil Kamal Dutta.

tite of bone like Ca^{2+} and Zn^{2+}. Gold has extensive application in catalysts, electronics and medicines, which when disposed in an uncontrolled manner, can be leached into waste water and pollutes the environment e.g. Au(III) ions can disrupt the molecular structure of the cell by interacting with phospholipid bilayer and thus affect the ion channel[13]. Palladium is more frequent in chemical and automobile industry for its catalytic application and thus Pd-based waste materials is a major contributor in heavy metal pollution[14]. Pd(II), in even low doses can cause allergic reaction in human beings[15]. Use of platinum has escalated in recent years due to its multiple applications from ornaments to microelectronics[16]. Platinum is believed to induce several allergic reactions which include urticaria, itching of skin, eyes, and nose, watering of the eyes, sneezing, rhinorrhoea, coughing, wheezing, and dyspnoea, and also it is a potential nephrotoxic and causes tubule damage[17,18]. Once emitted from the respective sources, these metals in various chemical camouflage enters the biota and significantly perturbs the ecosystem. For example, Pawlak *et al*. has discussed the fate of platinum group metals in his review article[19].

Precious elements (Ag, Au, Pd and Pt), in various forms, are available in environment (air, water), archaeological artefacts, geological materials (soil, rock, ore), industrial waste and food materials, in different concentrations. All these sources can contribute to the availability of these metals in the environment beyond their toxic levels. The current and evolving techniques have been directed to detect these elements in a convenient and faster way to ensure environmental consciousness in the society. Spectroscopic techniques such as atomic absorption spectroscopy (including its different variants like FAAS, CVAAS, GFAAS, HGAAS), optical emission spectroscopy, etc. have long been applied in "chemical autopsy" of the samples for trace elements, while spectrometric methods such as ICPMS analyses elements to trace and ultra-trace level, in addition to non-destructive methods like XRD and SEM-EDS, have played vital role (Fig. 1)[20–25]. Conventional techniques such as UV-Visible spectrophotometry, FT-IR, NMR and mass spectrometry also have been applied to detect metal ions in solution and consequently have not been discussed here in details. It is noteworthy that these techniques are destructive in nature and requires either digestion or processing of the solid samples. While some techniques bear the advantage of rapid analysis with high throughput, others can provide very low detection limit with enhanced precision. But none of the methods bear the suitability to analyze each and every other kind of sample due to their intrinsic nature of detection and physical capabilities. This implies while ore and rock samples needs to be completely degraded with fusion or acid digestion to extract the metal from surrounding matrix, archaeological samples have to be analyzed without destroying the sample with non-destructive analytical methods. In many cases the advantages of two methods have been exploited by application of hyphenated techniques SEM-EDS, HPLC-ICPMS, etc. In such cases, analysis becomes sample specific and case specific[23,26]. Moreover, relatively faster method where fluorescence and colorimetric technique is used, with the help of a chemosensor, is also frequently resorted to in order to avoid heavy instrumental involvement[27]. And therefore, discussion of different methods of analysis addressing samples of different background is needed.

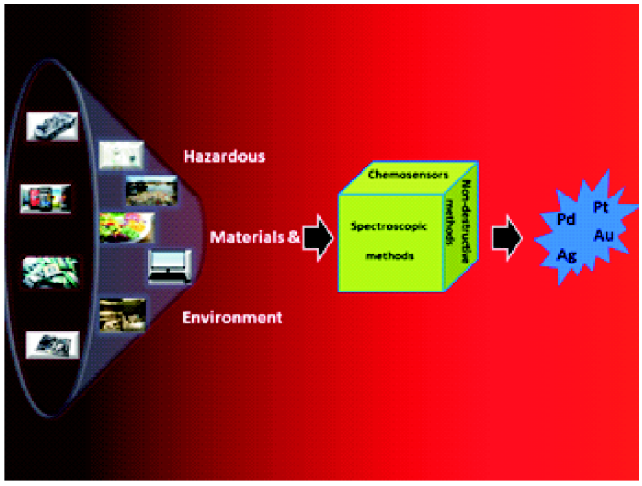

Fig. 1. Schematic diagram of various precious metal sources and their analysis by different techniques.

In this review, different analytical techniques, in accordance to the nature of samples to be analyzed, have been discussed in details covering recent and relevant literatures. Three broad categories, viz. spectroscopy (mainly AAS) in addition to a preconcentration technique, chemosensors and non-destructive techniques are presented with literature study encompassing broad spectrum of modern techniques. Spectroscopic techniques were well-explored and to understand its application with a comparatively new method of preconcentration to lower down its LOD and improve performance have been discussed. A critical overview on the nature of absorbents necessary for different precious metals is

presented. Even many natural products possess good adsorption properties and hence contribute in solid phase extraction (SPE). The influence of several parameters like pH, time, amount of adsorbing material, re-usability, etc. has been discussed. The complete extraction process used in spectroscopic determination is a fool-proof method. Chemosensors, on the other hand, are very good agents to detect precious metals and helps to avoid hazardous acid treatment and avoid complicated instrumentation for analysis. Their application is however dependent on the chemical groups, ligating donor atoms and the pH at which they exhibit the change in color. The aforementioned parameters were addressed in details for each examples cited to provide a detailed overview of the method. Many times it is required to avoid excessive use of corrosive acids as in digestion technique for spectroscopic analysis and other toxic reagents or solvents, which are otherwise a potential threat to the environment. For such instances, non-destructive methods provide valuable option through sophisticated and advanced instrumentation. Different techniques in this category have been explored here with suitable literature. Each technique shows differential affinity for different kind of sample and different elements. The suitability of the methods was compared in terms of their merits and demerits with respect to the determination of precious metals. Most detection limits given in text and tables refer to concentrations in ppm, ppb, etc. in sample digests or concentrates not in original solid samples. To the best of our knowledge, no such review has been specifically devoted to the determination of the precious metals mainly, silver, gold, palladium and platinum, in a source specific and technique specific manner. The expanse of applicability of each technique is also discussed for precious metal analysis.

2. Spectroscopic analysis

Instrumental methods which play a pivotal role in determination of elements including precious metals, encounters the limitations of insufficient sensitivity and interference from matrix elements. Although several groups have dealt with conventional techniques such as FAAS, ETAAS, ICPMS, ICPOES, etc., in determination of trace level precious metals[28–33], and several detailed reviews have been compiled[34–37], modern preconcentration methods are necessary to aid the available spectroscopic and spectrometric techniques for determination of ultra-low level concentration of elements by bringing the elemental concentration range within the range of instrumental determinations. Therefore, such comparison of mere instrumental methods has been replaced with a comparative account of a versatile preconcentration technique in purview of treating different kind of samples for precious elements.

Several preconcentration techniques have been applied for analytical purpose such as liquid-liquid extraction[38], cloud point extraction[39], SPE[40], coprecipitation[41], electrodeposition[42], etc. Amongst the available methods, SPE works comparatively well for the precious metals which are found in very low concentrations from various sources such as environment, geological, electronic waste materials, etc.

In this method, a solid phase is used to selectively extract the target element from a liquid phase followed by a desorption/dissolution step, and in the process concentrates the analyte amount for facilitating the analysis/determination. This method has the advantage of being simple, comparatively cheaper, reproducible, convenient, faster, sensitive and efficient with high concentration factor compared to other methods. Several classes of materials have been successfully tested for preconcentration, separation and determination of precious elements such as silica-based resins, carbon-based materials, nanoparticles, MOFs and biosorbents. Each class of materials have been dealt with citing relevant recent examples separately so that the readers have the scope of classifiably choosing their material of interest according to the requirements.

Modified silica and resin derivatives have long been explored in inorganic and analytical chemistry owing to its structural properties, morphology, reactivity, availability and low cost. Tuzen *et al.* reported on the SPE of Au(III) ions by Dowex M 4195 followed by determination of the concentration by flame atomic absorption spectroscopy[43]. The surface functional group of the resin is amine (-NH_2) group capable of ligating with precious metal ions. The study was done on soil, sediment and mine samples. The effect of pH, flow rate, sorption capacity and interfering radicals were studied. Good recoveries were observed in the pH range 2–8 with sorption capacity of 8.1 mg/g. Interfering radicals showed little effect on the metal (Au) ion recovery with Cl^-, NO_3^-, K^+, Mg^{2+}, Fe^{3+} and Cu^{2+} showing the maximum effect. The detection limit of the optimized process was found to be 1.61 ppb. The chelating resin could be reused even after 100 cycles.

Mladenova *et al*. reported on a novel sorbent material based on cysteine modified silica gel for enrichment and determination of noble metal ions such as Au(III), Pd(II) and Pt(II)/Pt(IV)[44]. The new sorbent harnesses the thermochemical stability and mechanical robustness of silica support and the diverse donor/complexing property of cysteine viz., O-, S- and N- donor sites for complexation of various metal ions. The material showed quantitative sorption in the range 93–97% and good stability even after 500 cycles. The studies were performed at pH range 1–6 and proposed that the chlorocomplexes of the noble metal ions ($AuCl_4^-$, $PdCl_4^{2-}$, $PtCl_4^-$ and $PtCl_6^{2-}$) selectively binds to thiol group of the sorbent owing to the favorable soft-soft interaction as predicted by hard and soft acids and bases principle. The adsorption of the non-noble transition metal cations was enhanced at increasing pH due to the accessible hard coordinating carboxylate site of the sorbent at higher pH, thereby enhancing interference with pH. The high complexation rate, thus high sorption rate leads to a loading half time of 2–4 min for the noble metals. The average sorption capacity per gram of the sorbent was found to be 152 mg Au(III), 86 mg Pd(II) and 146 mg Pt(IV). The best eluent was 0.1 *M* thiourea in 0.1 *M* HCl, which showed high recoveries in the range 95–99%. Sorptions of metal ions were studied in river water, sea water, copper concentrates and soil samples to establish the diversity of the process. The preconcentrated ions were analyzed by either ETAAS or ICPOES. The detection limit of 2 and 6 ppb for Au in copper ore/concentrates samples using ETAAS and ICPOES, respectively were achieved. Behbahani *et al*. demonstrated the use of MCM-41 modified with 3,4-dihydroxybenzaldehyde for simultaneous separation and preconcentration of Cu, Ag, Pd and Au ions, and their measurement by FAAS[45]. Influence of pH, flow rates, interfering ions and sorption capacity were studied. Optimum retention was found to be at pH 5 with effective elution with HCl/thiourea was found at effective flow rate 0.5–2 ml/min. Simultaneous quantitative recoveries were obtained for sample volume up to 1700 ml with preconcentration factor of 567. Interfering ions had negligible influence on the sorption capacity at pH 5. The method was validated with analytical results of reference material (RM) and also determination of the elements in water and soil samples. Detection limit of 0.03, 0.5, 0.08 and 0.09 ppm, and the adsorption capacities of 130, 160, 155 and 290 mg/g, was observed for Cu, Ag, Pd and Au respectively. The recoveries were more than 97% for the elements. Awual *et al*. reported on adsorption and recovery of gold from urban mining waste, on inorganic silica modified with 6-((2-(2-hydroxy-1-naphthoyl)hydrazono)methyl) benzoic acid (HMBA) and consequent determination of the element with ICPAES[46]. SEM and TEM were applied to describe the structural detail of the porous material including pore size, which indicated retention of the ordered structure after immobilization of HMBA. Study on operating pH showed that the material exhibit optimum sensitivity and selectivity at pH 2. The sorbent showed high sorption capacity of 203.42 mg/g and a detection limit of 0.11 ppb could be achieved. Elution was carried out with acidified thiourea. The interfering radicals showed little influence on the sorption behaviour of the sorbent in the presence of 10-fold concentration of competing ions such as Cu^{2+}, Mg^{2+}, Hg^{2+}, Pd^{2+}, Ca^{2+}, Pt^{2+}, Ru^{3+}, Ni^{2+}, Al^{3+}, Co^{2+}, Fe^{3+}, $Cr^{3+}$and Bi^{3+}; however, a 50-fold concentration of interfering radicals showed a profound deviation (15%) on Au(III) sorption. Au(III) sorption decreased with increase in pH. The high selectivity of Au(III) sorption was attributed to the strong binding of nitrogen atom of the HMBA moiety.

The applications of carbon and carbon based materials have gained immense attention due to their availability, chemical attributes and ease of modification to suit the purpose. The adsorption capacity and selectivity of the aforementioned materials paves way for its use in sorbents. Moreover, tailoring of the materials is also possible with different surface modifications. Tu *et al*. presented one such example where activated carbon was chemically modified with ethyl-3-(2-aminoethylamino)-2-chlorobut-2-enoate and used in the SPE of Au(III), Pd(II) and Pt(IV) ions from aqueous solution and their determination by ICPAES[47]. The influence of pH, eluting solution, flow rate, interference, etc. was studied in details. The synthesized ethyl-3-(2-aminoethylamino)-2-chlorobut-2-enoate modified activated carbon was studied by FT-IR, elemental analysis and photoelectron spectroscopy. pH was varied from 1–7 and found that the maximum recoveries was seen at pH 1. At lower pH, the formed chloro-anionic complexes of the precious metals bind to the protonated amine group of the organic moiety of the adsorbent by ionic interaction, and favor their separation without much interference from other ions. It was also found that 2 ml of the eluting solution (HCl/thiourea) at 2 ml/min recovered the metals quantitatively with an enrichment factor of 125. The sample volume of 250 ml was standard and lead to >95%

recovery. The maximum adsorption capacity and detection limits for Au(III), Pd(II) and Pt(IV) were 305, 92 and 126 mg/g and 5, 11 and 9 ppb, respectively. Reproducibility was observed even after 10 cycles of experiments. The method was validated with the analysis of the reference materials GBW07293 and NIST SRM 2557 with satisfactory results. Another example of the carbon based material is the oxidized form of graphene (2-D sheets of carbon with atomic thickness) known as graphene oxide containing epoxy, hydroxyl and carboxyl groups which can coordinate to metal ion via O-donor. Kazemi *et al*. reported on the preconcentration of gold ions in water and wastewater samples and a reference material (CCU-1b, copper flotation concentrate), by magnetic graphene oxide prepared by one-step coprecipitation method, as the first example of dispersive solid phase microextraction for gold[48]. The as-synthesized magnetic graphene oxide was characterized by FT-IR, XRD and SEM for its composition and structure. Although recovery of Au(III) was satisfactory up to pH 7, a pH of 2 was chosen to eliminate interfering effect of other radicals. Acidified thiourea was used as eluting solution. The separated gold ions were analyzed by FAAS. Optimum sample volume for maximum extraction efficiency was 50 ml. The capacity of the sorbent was 9.8 mg/g and the material was effective after 10 cycles of operations. The detection limit of 4 ppb with enrichment factor of 500 was observed. Furthermore, Moghaddam *et al*. reported on applicability of carbon nanotube, a form of graphene rolled into tube, for separation and hence determination of Au(III) by ETAAS with low detection limit and high enrichment factor[49]. The special structural orientation of CNTs provides for its high surface area, high adsorption capacity and hydrophobicity, and thus they are attractive candidates for removal and separation of different substances. An oxidized MWCNTs modified with 2-(5-bromo-2-pyridylazo)-5-(diethylamino) phenol was prepared and characterized by FT-IR and SEM for composition and morphology. An acidified thiourea with 3 ml HCl (2 *M*) and 2 ml thiourea (1 *M*) was used as eluting solution and a favorable pH of 6 was selected after several tests. Additionally, a sample flow rate of 3 ml/min and eluting solution flow rate of 1.5 ml/min was selected for optimized results. An enrichment factor of 200 was achieved with final eluent volume of 5 ml and breakthrough sample volume of 1000 ml. Reliable separation was observed even after 40 cycles. A low detection limit of 31 ppt and sorption capacity of 4.15 mg/g could be achieved with this modified MWCNT. The method was successfully tested on water samples, human hair, human urine and standard reference material.

Apart from the carbon based materials, some hybrid material systems combining advantageous properties of different systems to selectively separate precious metal ions have been applied to achieve better results. A polypropylene amine dendrimers (POPAM)-grafted multi-walled carbon nanotubes (MWCNTs) hybrid material was prepared by Behbahani *et al.* and applied for the preconcentration of Au(III) and Pd(II) ions in environmental and biological (fish and shrimp) samples; analyzed by FAAS[50]. The terminal group of the dendrimer provide ample scope for modification of functional property on the nanocomposite material. The as-synthesized hybrid material was analyzed by TEM, NMR, TGA, FT-IR and XPS. An optimum pH of 3 was chosen for the separation purpose wherein the ion pair formation occurs between chloro-anionic complex of precious metals and the protonated amine group of the dendrimer. No significant interference of other ions was observed at the selected pH. A breakthrough volume of 900 and elution volume of 2.5 ml provided an enrichment factor of 360. The adsorption capacity of the material for Au(III) and Pd(II) were 92 and 74 mg/g respectively. The detection limit for Au(III) and Pd(II) were 0.08 and 0.12 ppm respectively. The method was validated by analysis of reference material NCS DC 73323 and mines stone samples. Jalilan *et al.* reported on an engineered magnetic nanocomposite material for SPE of Ag(I), Au(III), Pd(II) and Pt(IV) with satisfactory selectivity even at high interfering ion concentration[51]. The MGO composite, made from silica coated and Fe_3O_4 decorated graphene oxide and polypyrrole-polythiophene copolymer, was characterized for structure and composition with SEM, TEM, VSM, FT-IR, EDS and TGA. The copolymer was selected in order to have sufficient soft ion coordinating sites enriched in S- and N- donor atoms for a rapid and selective method. The polypyrrole-polythiophene copolymer additionally provides the advantage of low cost, less toxicity, convenient synthetic pathway and coordinating ability towards the analytes. In this work the advantage of high surface area of graphene is combined with reactivity/selectivity of the copolymer and provided mechanical support over silica and the Fe_3O_4 particles introduced for cleaner separation based on magnetic technique in a very cautious manner. It is noteworthy that although the individual components show promise for coordination with

precious metal ions, they possess several demerits like poor chemical strength and physical instability for efficient separation/preconcentration. The sorption capacity of the nanocomposite for Ag(I), Au(III), Pd(II) and Pt(IV) were 49, 50, 45 and 50 mg/g respectively. The method was applied successfully on different samples and different matrices such as waste water (electroplating, radiological and photographical wastewater), sea water and road dust with impressive recoveries between 95.8 and 103%. The method was also validated with analysis of a reference material (Ore polymetallic gold Zidarovo-PMZrZ (206 BG 326)) by FAAS after separation with the nanocomposite. Detection limit for the analyte elements varied from 0.1–1.0 ppb.

MOFs are a relatively new class of materials which exhibit unique properties such as chemical stability, high surface area and tunable pore structure. They are solid crystalline substances composing of metal ions connected by organic ligand to form a 3-D framework. They are used for catalysis, drug delivery, gas storage, chemical sensing, etc.[52]. Therefore, MOFs are good candidates for adsorption of heavy metals from solutions selectively. A magnetic MOF [(Fe_3O_4-pyridine)/$Cu_3(BTC)_2$] was prepared and used for preconcentration of Pd(II) in water (river and mineral water), soil, sediment and fish samples and analyzed by FAAS[53]. The method was validated with the study of reference materials from Geological Survey of Iran. An optimization study was also performed assuming different variables viz., extraction time, pH, MOF amount, elution time, concentration of eluent, etc. Adsorption of Pd(II) increased with increase of pH due to the protonation of active sites at lower pH. A pH of 6.9 was chosen as the optimum acidic condition. 0.01 *M* NaOH showed maximum recovery without affecting the MOF structure and therefore it was selected as the eluting solvent. The process could withstand a sample volume of 1250 ml with 98% recovery and a preconcentration factor of 208. Sorption capacity of the material was 105.1 mg/g. The recoveries of Pd(II) ions varied from 98–102.6% for the different samples analyzed. The material showed high selectivity at pH 6.9.

A typically different way is to carry out the SPE of precious metals with natural ingredients or with the help of biosorbents, which facilitate for an efficient and low cost material, with nominal physical and chemical treatment[54,55]. While both inorganic and organic substances are available in the pool, organic materials have an extra edge of being easily available as high absorption by-products. Ju *et al*. reported on biosorption of Au(III), Pd(II) and Pt(IV) by a unicellular red algae *Galdieria sulphuraria*[56]. Over 90% of Au(III) and Pd(II) was selectively recovered from aqua regia based waste water containing high concentration of base metals (including Fe, Ni, Sn, Cu, Zn, etc.). The application of *G. sulphuraria* is due to the fact that it can tolerate harsh chemical environment and exhibit selectivity in sorption property. SEM-EDS and time-resolved ICPMS were used to determine elemental concentration in the cell without any treatment. *G. sulphuraria* showed more efficient removal of precious metals compared to *Chlorella vurgaris* at pH 2. A 30 min incubation time was sufficient to concentrate the metal ions in the cell. The chloride complexes of the precious metals bonded with the amine functionality on the cell surface. The sorbent showed a sorption capacity of 34 mg/g within 30 min for Au(III) ions. Acidified thiourea in the presence of ammonium ions resulted in selective elution of Au(III) and Pd(II) from the biosorbent. Recently, Losev *et al*. reported on pine dust and malt sprouts, treated with dimethylformamide, orthophosphoric acid, and carbamide[57], as effective biosorbents for SPE of non-ferrous, heavy and precious metal ions. The available active amine and phosphoryl groups on the biosorbents are responsible for separation of the analyte ions. It is important to note that such biosorbents are stable against dilute solutions of inorganic acid and alkalis. Sorbents with low degree of phosphorylation and high degree of amine functionality is efficient for precious metal preconcentration. A 10 min time was sufficient for ion extraction of Ag(I), Au(III), Pd(II) and Pt(IV) ions. The separation of the ions by sorbent material is attributed to the anion exchange and chelation process. It was shown that at elevated temperature (95°C) the removal of Pt increased due to pathway of primary chelation mechanism. A flow rate of 1–2 ml/min was sufficient to remove the Au(III) and Pd(II) ions, while a volume of 5 ml of acidified thiocarbamide (eluent) was enough for 99% recovery of the ions. The method was validated with certified reference material VT-1 and VP-2 (sulphide Cu-Ni ore) and the samples were finally analyzed with ICPOES.

A broad spectrum of different classes of materials have been categorically presented for the preconcentration and thus determination of precious metal elements according to the availability of the technique and material of choice. The purpose of this section was to provide a knowledge base

Table 1. Summary of the materials applied for preconcentration of precious metal ions for trace level analysis

Sorbent material	Samples analyzed	Ions separated	Sorption capacity (mg/g)		Analytical technique	Detection limit	Literature
Silica and resin based sorbents							
Dowex M4195	Soil, sediment and mines samples	Au(III)	8.1		FAAS	1.61 ppb	43
Cysteine-modified silica gel	River water, sea water, soil samples and copper concentrates	Au(III), Pd(II), Pt(II)/Pt(IV)	Au(III): 0.77 Pt(IV): 0.75	Pd(II): 0.81	ETAAS/ ICPOES	2 and 6 ppb for Au(III) by ETAAS and ICPOES respectively	44
MCM-41 modified with 3,4-dihydroxybenzaldehyde	Water and soil samples	Cu(II), Ag(I), Au(III), Pd(II)	Cu(II): 130 Au(III): 290	Ag(I): 160 Pd(II): 155	FAAS	Cu(II): 0.03 ppm, Ag(I): 0.5 ppm Au(III): 0.09 ppm, Pd(II): 0.08 ppm	45
Silica modified with 6-((2-(2-hydroxy-1-naphthoyl)hydrazono) methyl) benzoic acid	Urban mining waste	Au(III)	203.42		ICPAES	0.11 ppb	46
Carbon based sorbents							
Activated carbon modified with ethyl-3-(2-aminoethylamino)-2-chlorobut-2-enoate	Road dust, smelter sample and certified reference materials	Au(III), Pd(II), Pt(IV)	Au(III): 305 Pt(IV): 126	Pd(II): 92	ICPAES	Au(III): 5 ppb, Pd(II): 11 ppb Pt(IV): 9 ppb	47
Magnetic graphene oxide	Water, waste water and reference material	Au(III)	9.8		FAAS	4 ppb	48
MWCNTs modified with 2-(5-bromo-2-pyridylazo)-5-(diethylamino)phenol	Water samples, human hair, human urine and reference material	Au(III)	4.15		ETAAS	31 ppt	49
Hybrid systems as sorbents							
Polypropylene amine dendrimers (POPAM)-grafted multi-walled carbon nanotubes (MWCNTs) hybrid material	Environmental and biological samples (fish and shrimp)	Au(III), Pd(II)	Au(III): 92	Pd(II): 74	FAAS	Au(III): 0.08 ppm Pd(III): 0.12 ppm	50
A magnetic graphene oxide nano-composite, made from silica coated and Fe_3O_4 decorated graphene oxide and polypyrrole-polythiophene copolymer	Waste water, sea water, road dust and reference material	Ag(I), Au(III), Pd(II), Pt(IV)	Ag(I): 49 Au(III): 50	Pd(II): 45 Pt(IV): 50	FAAS	0.1–1.0 ppb	51
A magnetic MOF [(Fe_3O_4-pyridine)/ $Cu_3(BTC)_2$]	Natural water, soil, sediment, fish samples and reference material	Pd(II)	105.1		FAAS	0.37 ppm	53
Biosorbents							
An unicellular red algae *Galdieria sulphuraria*	Waste water	Au(III), Pd(II), Pt(IV)	Au(III):34 (30 min, 0.4–0.5 *M* dil. aqua regia)		SEM-EDS, time resolved ICPMS	–	56
Pine dust and malt sprout	Environmental samples	Ag(I), Au(III), Pd(II), Pt(IV)	Au(III):12.80	Pd(II): 6.15	ICPOES	–	57

and options available in the modern scientific arena when the limitation of detection limits and matrix interference hinder the determination of the precious elements.

3. Role of chemosensors

To avoid heavy instrumentation and lengthy concentration and digestion processes chromogenic methods have been widely applied and accepted for detection of many elements. Chemosensors are extensively used wherever applicable in order to reduce complicated extraction and concentration procedures which are chemically cumbersome and hazardous. Fluorescent sensors are efficient tools to detect metal ions at ppb and sub-ppb levels due to their selectivity and sensitivity. Therefore, the colorimetric and fluorescent techniques are extensively used to detect the precious metal ions like Ag, Au, Pd, and Pt ions[58–60].

3.1. Colorimetric sensor for detection of silver

Extensive research for colorimetric detection of silver ions has been devoted due to its suitable size and binding property to both hard and soft sites present in the ligand moiety. Sensors based on cyclic molecules with N,O,S-donor were successfully used with variation in their peripheral groups and side chain functionality and overall bulk. For example, naphthalimide derivatives **C1-C3** have detected Ag(I) ions selectively. Xu *et al*. reported naphthalimide derivative **C1** and **C2** as selective chemosensor for Ag(I) ion[61]. While **C1** exhibited turn-on fluorescence phenomenon with high fluorescent enhancement (nearly 14 fold) and a high association constant (1.24×10^5 M^{-1}) in CH_3CN-H_2O (1:1, at buffer pH = 7.4) solution resulting in a detection limit as low as 1.08 ppb, probe **C2** showed a comparatively poor binding parameter with Ag(I) corroborating the fluorescent enhancement role of carbonyl group present between the naphthalimide and [15]ane NO_2S_2 units. Probe **C3** was reported by Chen *et al.* in which the O atoms in ether **C2** is replaced by S atoms shows binding of both Hg(II) and Ag(I) ions in EtOH-H_2O (1:4) solution at buffer pH = 7.14[62]. Ag(I) ion resulted in a fluorescence quenching (ϕ = 0.04) due to intramolecular d-π interaction between Ag(I) and the fluorophore.

Not only complex cyclic macromolecules but comparatively simple compounds with suitable ligating nodes/points have also fared well in the scale of chemosensors due to their structural and operational simplicity. Arulraj *et al.* reported on a rather structurally uncomplicated species, based on thionine, as a turn-off fluorescence probe for detection of Ag(I) ions to attain a detection limit of femtomolar level[63]. The Ag(I) ion induces a turn-off fluorescence phenomenon by quenching the intensity of thionine at pH 7. Thionine contains a nitrogen heterocycle and two amine groups symmetrically disposed on two sides. The emission maximum was observed at 623 nm owing to the excitation of free thionine molecule at 598 nm. The probe can detect Ag(I) ion up to a detection limit of 0.5 ppq (parts per quadrillion) at around pH 7 (phosphate buffer solution). Silver being a soft cation, prefers softer donor sites for coordination such as sulfur and nitrogen. Here the amine nitrogen being more electron rich than the ring heteroatoms acts as the preferred binding site for silver ions. Other cations such as Co^{2+}, Cr^{2+}, Pb^{2+}, Cu^{2+}, Sr^{2+}, Ca^{2+} and Ba^{2+} produced negligible interference in the detection of silver confirming the selectivity of the probe. A 4-methoxy-*N*-((thiophen-2-yl)methyl) benzenamine chemo sensor was found to detect selectively Ag(I) ion over other ions such as Na^+, K^+, Li^+, Cu^+, Ba^{2+}, Cd^{2+}, Co^{2+}, Cu^{2+}, Fe^{2+}, Hg^{2+}, Mn^{2+}, Ni^{2+}, Pb^{2+} and Zn^{2+}[64]. The probe work by an intramolecular charge transfer mechanism, corroborated by time-dependent density functional theory (TD-DFT) calculations, in MeOH-H_2O (1:1 v/v) with a detection limit of about 0.5 ppm.

Many a times metal-loaded complex have been used for detection of Ag(I) ion. Schmittel and Lin *et al.* reported two complexes **C4** and **C5**, based on an aza-dithia-dioxa crown-ether-decorated Ir(III) and Ru(II) ions[65,66]. Both the complexes showed selective binding property with respect to Ag(I) ions as indicated by their luminescence response. The iridium complex **C4** showed a higher luminescence enhancement factor (10 times) than the ruthenium complex **C5**. Probe **C4** showed an evident red shift (~36 nm) in its emission wavelength on binding Ag(I) ion and a pronounced enhancement. It should be mentioned that addition of Hg^{2+} lead to quenching of emission of **C4** owing to electron- or energy-quenching effect of the unbound Hg^{2+} ion. Two calixarene derivatives **C6** and **C7** bearing crown ether and an azacrown ether as the binding were developed by Kim *et al*.[67,68]. A fluorescence quenching of **C6** was observed in MeOH via a photo-induced electron transfer (PET) process. Ag(I) went to the azacrown site indicated by the fluorescence enhancement and the addition of K^+ ion led to the fluorescence quenching which is proposed to fit into the crown ether loop and expel the Ag(I). Ag(I)-**C7** complex showed a decrease in fluores-

cent intensity when Cs^+ which nicely fits into the crown-6 cavity and expels the Ag(I) ion. A selenium loaded coumarin complex bearing a Se_2N unit was synthesized and studied with respect to its binding property to Ag(I) ion by Huang *et al.*[69]. The probe showed high sensitivity and fluorescent enhancement (4 fold) due to inhibition of the PET quenching process in EtOH-H_2O (1:1) medium. The detection limit was estimated to be around 6 ppb. A zinc loaded phthalocyanine derivative **C8** was applied as a fluorescent sensor for Ag(I)[70]. The binding of Ag(I) to **C8** in tetrahydrofuran led to enhanced intensity of the coordinated species (642 nm) and gradual disappearance of the absorption band of **C8** at 688 nm and the accompanying change of color from blue-green to black-dark green which indicated the binding of Ag(I) to the phthalocyanine derivative **C8**. A terbium(III)-thiacalix[4]arene complex **C9** was reported by Iki *et al.* for the detection of Ag(I) with an impressive detection limit of less than 1 ppb[71]. The intensity of **C9** at 544 nm showed a linear surge as the Ag(I) concentration was increased owing to the formation of the ternary complex **C9**-Ag(I). Addition of other transition metal ions like Co^{2+}, Ni^{2+}, and Pb^{2+} caused very slight change in the intensity while Fe^{3+} and Cu^{2+} led to decrease in intensity of the original fluorescence to the tune of 57% and 67% respectively. Addition of Cd^{2+} led to increase in fluorescence intensity.

Detection of Ag(I) by application of nanoparticles (NP) and quantum dots (QD) have been the new trend with a number of research groups working on this area. A surface modified AuNP was applied by Lin *et al.* to detect Ag(I) and Hg(II) ions[72]. The same NP aggregate could selectively detect Ag(I) ion in the presence NaCl and EDTA at a low concentration of around 11 ppb while the determination of AgNP could be done at a detection limit of ppt level. This probe was applied to detect Ag(I) and AgNP in drinking water at a minimum detection limit of 0.03 ppm and 0.1 ppt respectively. Recently, Wang *et al.* and Selva Sharma *et al.* applied platinum and gold NPs respectively, for the detection of very low concentration of silver ions in solution[73,74].

Recently Zhao *et al.* reported a graphene quantum dots and *o*-phynylenediamine as nanosensor for Ag(I) ion detection[75]. The Ag(I) ions oxidizes the *o*-phynylenediamine to 2,3-diaminophenazine which shows strong fluorescence emission at 557 nm followed by a quenching of the signal of graphene quantum dots at 445 nm by a FRET mechanism.

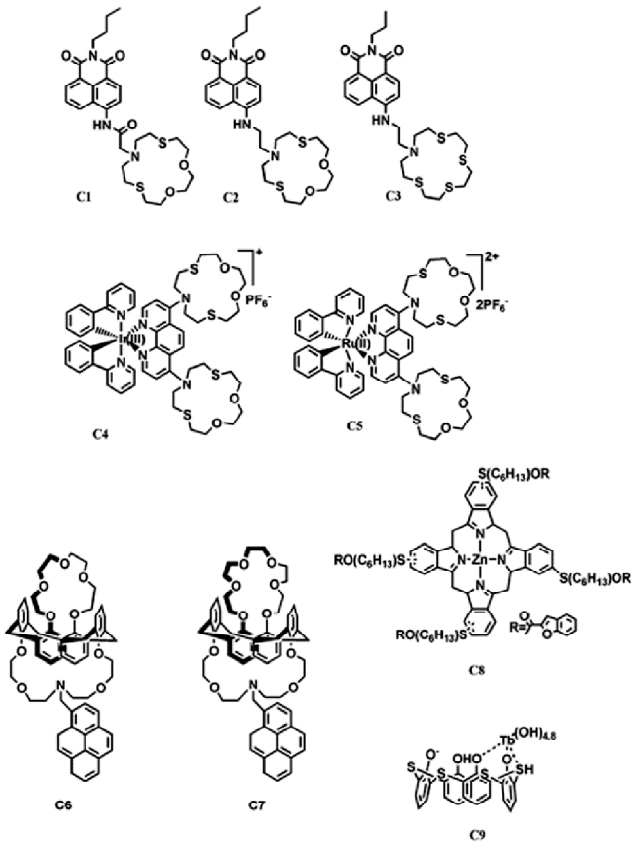

Fig. 2. Chemical structure of chemosensors **C1**-**C9**.

The application of the above probe led to a low detection limit of 28 ppb. CdTe quantum dots in the presence of L-cysteine have been found to act as a fluorescent sensor for Ag(I), Cu^{2+} and Hg^{2+} in the presence of suitable masking agents[76]. The analyte ions quench the fluorescence intensity considerably leading to detection of these ions. The presence of cysteine, which contains a thiol group, improves the fluorescence intensity by binding with the Cd^{2+} generating more radiative centers. The synthesized probe has been successfully applied in the determination of the ions in water, tea infusion, soda water, orange juice, and red wine.

The properties of silver to interact with a number of biomolecules have been exploited by analytical chemist to develop biosensors[77] or biomolecule-based sensors for detection of Ag(I). Park *et al.* harnessed the fluorescence property of a mismatched pyrrolo-dC (PdC)-modified duplex DNA to fabricate a fluorescence probe for detection of Ag(I)[78]. The probe showed high selectivity and specificity. Recently Miao *et al.* developed a highly selective regenerable DNA based

biosensor for Ag(I) ion detection and attained a low limit of detection of 0.01 ppb[79]. The specific cytosine-Ag(I)-cytosine structure controls the conformational change of the DNA probes on the electrode and the obtained electrochemical response is related to the Ag(I) concentration. Wu *et al*. compared the relative binding ability of Ag(I) with different DNA bases and their subsequent application in the DNA based probes for Ag(I) ion detection[80]. Sensors fabricated with DNA probes containing both adenine and cytosine was found to be ideal for this application. In contrast, probes containing both cytosine and thymine, independent of the location of the alkanethiol linker, did not respond to Ag(I). In another instance, a naturally occurring plant alkaloid was employed as a fluorescent probe for Ag(I)[81]. Ag^+ ions induced a fluorescence quenching over other metal ions such as Cu^{2+}, Zn^{2+}, Sn^{2+}, Ni^{2+}, Ba^{2+}, Bi^{2+}, Pb^{2+}, Co^{3+}, In^{3+}, Mn^{2+}, Fe^{2+}, Fe^{3+}, Li^+, Hg^{2+} and Ca^{2+} achieving a detection limit of around 1 ppm in a EtOH-H_2O (1:1, v/v) medium. A 1:1 complex between the probe molecule and Ag(I) was confirmed as indicated by ESI-MS and Job's plot analysis.

3.2. Colorimetric sensor for detection of gold

Gold as an ionic/atomic species have been applied in a number of ways right from nanotechnology to biotechnology and consequently its detection becomes a matter of concern to the people working in any major field.

Ever since Jou *et al*. reported the first functional fluorometric Off-On type probe **C10** for Au(III)[82] which was successfully applied for cell imaging of Au(III) reaching a detection limit of 63 ppb; a number of research articles have featured on the development of gold probe with different structural and functional variations[83-85]. Dong *et al*. developed a 1,8-naphthalimide based probe for selective detection of Au(III) and Hg^{2+} by a ratiometric fluorescent method which is one of its first kind[86]. Patil *et al.* synthesized a probe from fluorescein for detection of gold (Au(I)/Au(III)) based on an anchoring-unanchoring process[87]. The probe has an absorption maximum at 313 nm in CH_3CN/PBS buffer (1:1, pH = 7.4) with no absorption in the visible region. However, the addition of Au(I)/Au(III) ions to probe **C11** changed the color of solution to yellow (from colorless) which was persistent to naked eye. Appearance of a new band at 452 nm was observed with a large enhancement in absorption. The solution of probe in the same buffer solution (pH 7.4) exhibit negligible fluorescence, while addition of Au(I) ion induced a large increase in fluorescence. Other metal ions such as Ag^+, Ba^{2+}, Bi^{3+}, Fe^{3+}, Hg^{2+}, Ir^{3+}, K^+, La^{3+}, Mn^{2+}, Ni^{2+}, Pd^{2+}, Pt^{2+}, Pt^{4+}, Ru^{3+}, Sc^{3+}, Yb^{3+}, Zn^{2+}, Cd^{2+} and Cr^{3+} induced negligible fluorescence response making the probe highly selective. Cell imaging studies were successfully performed with living cell such as A549 lung cancer cells.

Park *et al*. developed a selective chemosensor for Au(III) based on the selective desulfurization of thiocoumarin to its oxo derivative in the presence of a masking agent N,N,N2, N2-tetrakis-(2-pyridylmethyl)ethylenediamine, which prevents the interference of heavy metal ions like Hg^{2+} which would otherwise compete in the desulfurization step[88]. The desulfurization was confirmed by ^1H NMR experiment. The same probe can also differentiate between two common oxidation state of gold (Au(I) and Au(III)); showing a selective response to Au(III) and almost no response to Au(I). Probe had absorption bands at 366 and 520 nm in a mixture of acetonitrile and acetate buffer solution (1:1, pH 4.7). With 20 equivalent of Au(III) or Hg^{2+} ions, the absorption band at 520 nm disappeared almost completely, and a new band at 463 nm developed and the color of the solution changed from pink to yellowish green. Detection limit was found to be around 12 ppb. Similarly, Yang *et al*. also reported on a probe for gold(III) depending on its ability to coordinate to cyano group[89]. The probe functioned well at physiological environment and possesses good cell permeability. Interference from a wide range of ions were studied and it was found that only HSO_3^- ion offered minor interference in fluorescence and UV spectra. When Au(III) was added, the absorption peaks at 552 nm gradually diminished and a new peak appeared at 600 nm accompanied by a color change of the solution from pink to brown. The shift in the absorption peak may be attributed to spin-forbidden metal ligand charge transfer (MLCT) (dp(Au)-p*(probe)) transitions. When the fluorescence study was performed in CH_3CN-HEPES buffer (1:1, pH 7.4), a fluorescence quench at 583 nm was noticed on Au(III) addition (from yellow to colorless) under illumination with a UV 365 nm lamp. The detection limit was about 0.1 ppm.

Elshehy *et al*. reported on an optical mesocaptor for selective detection of Au(III) at trace level by immobilization of a 6-hydroxy-5-(4-sulfonatophenylazo)-2-naphthalene-sulfonic acid disodium salt probe into the 3-D cubic mesostructures (pore size in μm range)[90]. The mesocaptor can be regenerated by eluting the adsorbed Au(III) with a stripping agents.

The high surface area and large pore diameter helps in ultratrace level detection of Au(III). By functionalization of the cubic mesostructures the size of pore can be engineered and applied in a wider variety of metal ion detection. The complexation of target ion with the probe is a function of pH of the solution and time. In the presence of high concentration of interfering ions, an uptake percentage of 73% was observed in the presence of 0.01 *M* EDTA used as masking agent for interfering Cu(II) radical at pH 7. Hence the optical mesocaptor shows excellent property in terms of stability, reversibility, selectivity, and sensitivity. Zuber *et al.* reported on detection of gold NPs through absorption and fluorescence studies depending on the size of the NPs and applied measurement apparatus[91]. The methods were investigated for detection of gold NP in ppb concentration level and the impact of size of NPs. Non-fluorescent I-BODIPY (4,4-difluoro-4-bora-3*a*,4*a*-diaza-*s*-indacene) was used in the fluorescence study as a fluorophore. A fluorescence peak at 510 nm was observed whereby the peak intensity increased with increase in concentration of gold NPs. The detection limit could go down to 74 ppb. The LOQ of fluorescence measurements decreased with decreasing gold NP size. Absorption studies showed that the peak maximum shifted from 514 nm for 5 nm NPs, through 519 nm for 20 nm NPs to 526 nm for 50 nm NPs. The differences in the frequency of surface plasmon oscillations of the free electrons is the main reason for the shift towards longer wavelength with the increase in NP size while the enhancement in absorbance with NP size is due to the enhanced mean free path of the electrons in the larger NPs. The absorption peak showed a linear increase with gold concentration, which indicates that gold NPs obey the Lambert-Beer law. The absorption method tends to give lower LOQ of larger NPs while portable fluorescence analysis would give lower LOQ for smaller NPs. The adopted methods assure the potential for their applications in geological and biological studies. Shahat *et al*. reported on a potential Thiomichler's ketone and mesoporous silica support for detection of Au(III), Ag(I), Pd(II) and Hg(II) with a detection limit up to about 10 ppt[92]. The probe material had a good shelf life. The absorption spectra of the metal-TMK aggregate indicated that the sulfur group of the TMK ligand binds to the metal ions to form complexes. The color intensity of the $[metal\text{-}TMK]^{n+}$ complexes at the specific wavelengths increased in a linear correlation to the analyte concentrations up to the maximum plateau. No considerable interference was observed for large amount of alkaline metals or alkaline earth metal ions. Moreover, common anions which were supposed to hinder the detection such as Cl^-, NO_3^-, HCO_3^-, CO_3^{2-}, SO_4^{2-}, SO_3^{2-} and PO_4^{3-} had negligible effect on the TMK sensor. These anions were tolerated at concentrations of up to 200 times the concentrations of the analyte ions (Hg(II), Ag(I), Au(III), and Pd(II)) promising the selectivity of the method.

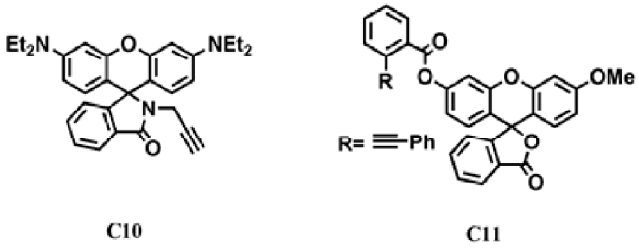

C10 C11

Fig. 3. Chemical structure of chemosensors **C10** and **C11**.

3.3. Colorimetric sensor for detection of palladium

Palladium undergoes a number of addition/catalytic reaction which in turn can be used to design its detection. Palladium is stabilized in +2 oxidation state (d^8 system) although its zero state is also maintained in many coordination complexes. They favor coordination number 4 and forms favorably square planar complexes. They show low affinity for "hard" ligands (F- and O) and show a preference for π-bonding ligands.

Koide and co-workers have reported on a fluorescence based **C12** (turn-off) for detection of palladium based on the palladium mediated Tsuji-Trost reaction[93]. $NaBH_4$ has been used to reduce Pd(II) to Pd(0). The adopted condition also allows detecting Pd in presence of sulfides which sometimes become a hurdle due to competitive binding. Jun *et al.* reported a rhodamine B derivative **C13** which exhibit a turn-on fluorescence and color changes[94]. A reducing agent $[(t\text{-}Bu)_3PH]BF_4$ converts $PdCl_2$ into the Pd(0) and aids in the catalytic process. No interference from Zn^{2+} and Al^{3+} species was observed in palladium detection. The probe also does not respond to Pt(II) species which co-exist with Pd in ores and interferes with Pd(II) detection[95]. Li *et al*. studied the detecting capability of different modified rhodamine derivatives in term of palladium sensing[96]. Introduction of allyl group in the spirolactam ring of rhodamine derivative and a terminal methyl group in allylidene-hydrazone ligand part led to enhanced selectivity of the sensor molecule **C14**. The elec-

tron donating methyl group assisted in adjustment of the electron density of the species. Pd(II) induced a high fluorescence enhancement and thus it could be detected by colorimetric and fluorometric method with little interference from common cations and other platinum group elements (PGE). A 2:1 stoichiometry between probe and Pd(II) is indicated from Job plots and TOF-MS results. A detection limit of about 20 ppb is reported. The Schiff base portion is attributed to the sensing property of the compound with the alkene group mainly being responsible for the adjustment of electron density, stereo effect and binding property leading to better selectivity of the probe.

Liu *et al*. reported a 2,6-dithienyl-4-phenylpyridine-containing conjugated polymer for selective sensing of Pd(II) and Pt(IV) in aqueous solution[97]. A 80% reduction in intensity was observed which is attributed to aggregation-induced fluorescence quenching which was confirmed by fluorescence anisotropy methods. No obvious change of fluorescence signal was observed in presence of other metal ions such as Ag^{+}, Ca^{2+}, Cd^{2+}, Co^{2+}, Cu^{2+}, Fe^{3+}, Hg^{2+}, Mg^{2+}, Ni^{2+} and Zn^{2+} thus assuring the selectivity and sensitivity of the probe. A detection limit of less than 0.1 ppm was observed for both Pd(II) and Pt(IV) species.

While metal organic frameworks (MOF) have been in the horizon of modern chemistry for quite some time now, their application in sensing of palladium metal ions have caught recent attention. He *et al.* reported ASMOF-5 to exhibit good sensing response to palladium and harnessed it for the detection of the metal[98]. The MOF is constructed out of a multifunctional building block of 2,6-dithioalloxyterephthalic acid containing both thioether and alkene functionality. The sulfur containing aromatic core possess intense photoluminescent property while the alkene group acts a π-donor/π-acceptor moiety helping in preferential binding to noble metals like palladium and platinum. The soft metals like Pd(II) and Pt(II) also interact with S-center and exhibit quenching effect. Pd species for example shows an orange-red color and can be colorimetrically detected by this MOF. Raman spectra of the Pd(II) treated MOF shows a band at 372 cm^{-1} characteristics of Pd(II)-olefin stretching frequency. Sub-ppm level of palladium can be detected and this process is not hindered by other metal ion concentration at low level e.g. 5 ppm. Due to the stark color change in palladium, it can be distinguished in presence of Pt^{2+}, Ir^{3+}, Ru^{3+} and other metal ions.

3.4. Colorimetric sensor for detection of platinum ions

Platinum, like palladium, shares similar chemistry in terms of coordination and binding ability. Therefore, its detection can be accomplished using similar reaction mechanism.

Similar to palladium the participation of platinum in Tsuji-Trost reaction was investigated and the same was employed for the detection and quantitative determination platinum in various samples. A Pt-catalyzed deallylation reaction was reported by Garner *et al*. on **C15**, which acted as the probe for Pt detection[99]. Pt(0) is believed to the main participating species and therefore a reducing ligand Ph_3P was used for *in situ* reduction of any Pt(II)/Pt(IV) species in medium to Pt(0). The conversion of **C15** to a fluorescent compound was achieved by the reaction of Pt(0) with **C15** in aqueous medium at pH 7-9. A detailed study of pH dependence of the reaction showed that the conversion is best carried out at pH 7 (3.5 times faster than pH 10) and a very poor progress observed at pH 4. A detection limit of 10 ppb could be achieved for *cis*-platin samples. Kim *et al.* reported a rhodamine triazole-based fluorescent chemosensor **C16** for the selective detection of platinum ions in aqueous solutions[100]. The probe consisted of dual binding unit of a hydroxamate and a triazole and shows high selectivity and sensitivity toward Pt(II) over other metal ions in aqueous medium. Probe **C16** does not show any color or fluorescence

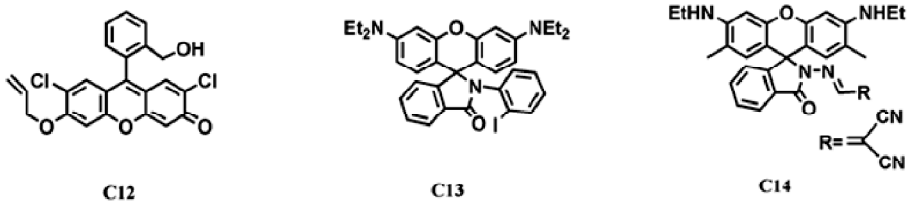

C12 C13 C14

Fig. 4. Chemical structure of chemosensors **C12**-**C14**.

in H_2O (DMSO 1% v/v) indicating that it exists in the spirocyclic form predominantly. On treatment with Pt(II) ions, the probe exerts strong fluorescence at 562 nm in H_2O (DMSO 1% v/v) and accompanying a change of solution from colorless to pink-red color. Probe **C16** could be used for sensing Pt(II) ions in the pH 5–9 range.

In an effort to improve upon older probes[99,100], for platinum and to cater to the detection of Pt(II) species in an intracellular environment, Montagner *et al.* developed a Rhodamine B based molecule containing a dithiocarbamate moiety[101]. The dithiocarbonyl bond bound to Pt(II) and induced a *trans* effect in the complex thereby making the reaction with spirolactam motif very facile making way for a turn-on fluorescence and subsequent detection of Pt(II). The probe was stable over a large pH range of 3.5–12 making it compatible with physiological conditions. A strong fluorescence response at emission wavelength 584 nm was recorded with a 65-fold enhancement. Job's plot analysis confirmed a 1:1 complex of probe with Pt(II). Interference from other metal ions such as Na^+, K^+, Mg^{2+}, Cu^{2+}, Ni^{2+}, Zn^{2+}, Fe^{2+} and Fe^{3+} was negligible even at high concentration of first three ionic species present *in vivo* corroborating the selectivity of the probe. Another fluorescein-based dithiocarbamic acid containing probe **C17** was successfully applied by Shen *et al.* in order to selectively detect monofunctional Pt(II) in cellular environment[102]. Addition of one equivalent of (2-(aminoethyl) ethane-1,2-diamine)-chlorido platinum(II) witnessed a 70-fold change in fluorescence emission and a linear increase in fluorescence with the mole fraction of probe between 0 and 1 equivalent. Binding studies confirmed a 1:1 complex between probe and Pt(II). The selective response of probe towards monofunctional Pt is presumably due to the π-π stacking interaction upon the binding of two fluorophore molecules in the bifunctional case which would quench the fluorescence. The probe could detect Pt in presence of other transition metal ions and was applied in colorectal cancer cells to detect reactive Pt species. Photostability of the probe still remains a limitation to be addressed.

4. Non-destructive analytical techniques

4.1. XRF

X-ray fluorescence has played a very important role in the qualitative and quantitative determination of a broad range of sample from different backgrounds including geology, archaeology, environment and industry. The advantage of this technique lies in its relatively smooth operation, ease of sample preparation and fast action. In this technique, an X-ray beam strikes the sample which results in the ejection of electron from inner core orbital of the metal creating a hole and resulting in the excitation of the atom. This is followed by transition of an electron from higher shell to fill the vacancy and emits an X-ray in the process (Auger process), corresponding to the energy gap between the two states. Since energy of the orbital of each atom is unique, the characteristic radiation corresponds to a particular atom and this helps in its identification and quantification. The quantitative determination of the element is possible by analyzing the intensity of the X-ray emitted by the atom.

Bédard *et al.* investigated a very important phenomenon called "nugget effect" commonly observed in geological ore samples which provides hindrance the determination of certain elements like Pd, Pt, Au, etc. by XRF and other analytical methods[103]. A number of sulphide and chromite bearing reference materials (MASS-1, MASS-3, WMS-1a, WMS-1, KPT-1, CHR-Pt^+ and CHR-Bkg) were analyzed by making pressed pellet of the samples. Considering six standard deviations for background, the size of the nugget that could produce a detection limit of 1000 ppm was found to be 10 μm (cubic) which is defined as the nugget threshold size.

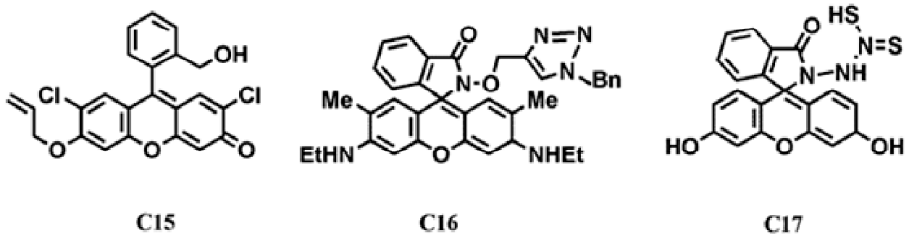

C15 C16 C17

Fig. 5. Chemical structure of chemosensors **C15**-**C17**.

Table 2. Comparison chart for detection of precious metals by chemosensor/probe

Chemosensor/probe*	Detection limit/range**	Literature	Chemosensor/probe*	Detection limit/range**	Literature
Detection of silver					
Naphthalimide derivative	1.08 ppb	61	Terbium loaded thiacalix[4]arene	0.35 ppb	71
Thionine-based chemosensor	0.5 ppq	63	Surface modified Au nanoparticle	ppt level	72
4-Methoxy-*N*-((thiophen-2-yl)methyl) benzenamine chemosensor	0.5 ppm	64	Graphene quantum dots and *o*-phynylenediamine	28 ppb	75
Aza-dithia-dioxa crown-ether-decorated Ir(III) ions	ppm level	65	CdTe quantum dots	0.5 ppb	76
Calixarene derivative with crown ether	ppm level	67	Modified duplex DNA	1 ppb	78
Selenium loaded coumarin complex	6 ppb	69	DNA based biosensor	0.01 ppb	79
Zinc loaded phthalocyanine derivative	ppm level	70	Berberine, a natural alkaloid	1 ppm	81
Detection of gold					
Rhodamine-alkyne derivative	63 ppb	82	Fluorescent Red GK	0.1 ppm	89
1,8-Naphthalimide based probe	20 ppm	86	Modified 3D cubic optical mesocaptor	8 ppb	90
Fluorescein based sensor	1 ppm	87	Non-fluorescent I-BODIPY (4,4-difluoro-4-bora-3*a*,4*a*-diaza-*s*-indacene) probe	74 ppb	91
Thiocoumarin derivative in the presence of a masking agent N,N,N2 ,N2 -tetrakis-(2-pyridylmethyl)ethylenediamine	12 ppb	88	Thiomichler's ketone on mesoporous silica support as sensor	10 ppt	92
Detection of palladium					
Allyl ether based probe	2.6 ppb	93	2,6-Dithienyl-4-phenylpyridine-containing conjugated polymer	0.1 ppm	97
Rhodamine B derivative	110 ppb	94	ASMOF-5	Sub-ppm level	98
Detection of platinum					
Allyl ether derivative	10 ppb	99	Rhodamine B based molecule containing a dithiocarbamate moiety	2 ppm	101
A rhodamine triazole-based fluorescent chemosensor	0.02 ppm	100	Fluorescein-based dithiocarbamic acid containing probe	—	102

*In case of similar probes, only representative example has been incorporated.

**In certain cases, concentration figures were rounded off to nearest numerical figures.

For generalization and in order to tackle the worst-case condition, all the elements analyzed were presumed to show nugget effect. It was further concluded that in order to minimize the microhetereogeneity of the sample/reference materials the minimum effective test portion mass should not be in few grams to sub-gram scale but considerably large.

Rodrigues *et al.* applied XRF technology to the archaeological samples (silver coins) of Trajan to understand the metallurgy of the period, purity of the alloy and ore sources[104]. Coins plays a crucial role in enlightenment of the archaeologist on the scientific and socio-economic prospects of the concerned historical period and consequently their analysis has to be accurate and non-destructive. The analysis was further corroborated with SEM-EDS technique. Silver enrichment was observed at 100–150 nm near surface which was attributed to the corrosion of the samples. A prominent negative correlation of the two major constituent viz., copper and silver of the coins was observed, which indicates that copper was added to silver bullion after the cupellation process. XRF aided in the depth profiling of the coins and it was found that in one coin the percentage of silver varied from 90% to 95% in different layers.

Muchova *et al.* analyzed the bottom ash samples of municipal solid waste incinerators from the city of Amsterdam

and Ludwigshafen by XRF[105]. The electronic and electrical materials comprising the solid waste of the developed cities are believed to contain several precious metals like gold and silver in considerable amounts. XRF data revealed that the approximate concentration of about 100 ppm and 1500–4000 ppm was found for gold and silver respectively. On comparison, it was found that the bottom ash samples of Dutch and German city resembles each other in terms of heavy nonferrous and precious metals. It was also concluded that 0–2 mm fraction has contribution of electrical waste and >6 mm fraction derived its precious metal content from jewelry. Birloaga *et al*. investigated the extraction and recovery of the precious metals from electronic circuit boards with leaching method with thiourea which has a promise for better recovery rate and lower toxicity, followed by analysis with semi quantitative XRF method[106]. With the thiourea-Fe(III)-dil. H_2SO_4 mixture leaching, most of the Au was found to be leached out in the solution with negligible (below detection limit i.e. <0.1 ppm) amount of the element being present in the solid waste. It is noteworthy that a three step oxidative leaching process was applied for Au recovery. A decrease in Au and Ag concentration was observed in the third and fourth step of leaching probably due to cementation/precipitation in the presence of elements like Al, Zn and Cu in the solid material. A positive correlation between the concentration of the precious elements (Ag and Au) and number of leaching step was noticed. This method of leaching-cum-XRF quantification bears a potential for application in the waste management of electrical and electronic solid wastes and help in the development of eco-friendly and efficient technology for future industrial sustenance.

4.2. LA-ICPMS

One of the most successful hyphenated successful technique offering accurate and comparatively faster measurement is laser ablation inductively coupled plasma mass spectrometry. This instrument also works efficiently as a dating tool. In this method a laser beam (Nd:YAG laser) of suitable energy (generally at wavelengths 213 nm/266 nm) is targeted on to a sample surface (kept in a closed laser ablation cell) across a transparent window. The ablated material is transported to the plasma torch by the flow of helium or argon. Ions are generated in the plasma, which are further separated and analyzed by mass analyzer e.g. quadrupole, time of flight or sector field. The use of shorter wavelength laser beam leads to production of smaller particles and increase sensitivity and precision of the process. The pulse duration of the laser varies from nanoseconds to femtoseconds. The shorter duration pulse results in production of fine aerosols, which can be atomized by plasma conveniently and a femtosecond pulse provides a scope for non-matrix matched calibration of the instrument to obtain very good result. Energy of a typical pulse is around few millijoule. The technology offers an *in situ* measurement and very low detection limit (sub-ppb).

Bendall *et al.* applied LA-ICPMS in combination with EPMA for the study of the different gold sources of the Celtic gold coins to establish the historical facts of the period[107]. LA-ICPMS was used predominantly to detect 28 trace elements in the coin samples. Pt was found as a trace element that varied substantially in the coins and the determination of Pt/Au ratios indicated the gold sources of the coins. The correlation of Pt with Au showed that different sources of gold were exploited in the coinage material in the Bohemia/Moravia. The presence of Pt also confirms Hellenistic sources. Dating was done by the LA-ICPMS method. The $^{207}Pb/^{206}Pb$ and $^{208}Pb/^{206}Pb$ ratios were taken for internal precision as in the gold coins the amount of Pb is low and therefore a lack of precision on ^{204}Pb is observed. The plot of $^{208}Pb/^{206}Pb$ and $^{207}Pb/^{206}Pb$ shows that the coins over 70% gold lie in the mixing line, and are related to the Pb isotope field of the Alps or Aegean. It was concluded from lead isotope data that the coinage metal did not come from Middle Rhine/Moselle region, but were either recycled from old coins/artefacts or was obtained imported from Hellenistic and Alpine sources. Martinón-Torres *et al*. investigated the Muisca votive goldwork of Columbia with LA-ICPMS, pXRF and SEM with the perspective of detailing about the material science in study of archaeological artefacts[108]. Several features of the archaeological objects like skill of the artisan/era, technical criticalities and materials used were obtained by chemical analysis, which led to in-depth understanding of the historical period. Minor disparity arose in the major element (Au, Ag, Cu) mapping of the artefacts (analysis of Tenjo objects) between data obtained by pXRF and LA-ICPMS due to their sampling technique, and pXRF provided more consistent results. However, the selective surficial or depth profiling was only possible by LA-ICPMS and for minor and trace elements

LA-ICPMS results were discussed. Features like depletion gilding (absent in Muisca art) were prominent in some samples (O33811), which were presumed to be a side-effect of fire exposure rather than oxidative loss of copper. The use of argentiferous gold (gold with 18% silver, estimated as the percentage of the ratio of silver upon total concentration of Ag and Au) and copper metal was evident in the samples validated by the trace element analysis. Although some samples evidenced use of different batches of gold depending on the Ag/Au ratios and PGE content of gold. More recently, Sarah *et al.* reported on a detailed depth profiling study performed with LA-ICPMS on the ancient samples of silver coins taking its pros and cons into the account[109].

Avarmaa *et al.* assessed the industrial materials generated from copper extraction process by EPMA and LA-ICPMS[110]. While EPMA was used to study the major elements of matte and slag, LA-ICPMS assisted in the determination of trace element of the slag for precious metal distribution such as Ag, Au, Pd, Pt, etc. at 1250–1350°C. Since precious metals are essential by-products of copper extraction process, their analysis followed by recovery and recycling becomes an indispensable requirement of the metallurgy process. Moreover, the increasing bulk of the electrical and electronic industry brings in heavy demand of conducting materials like copper. LA-ICPMS took the detection limit of trace elements in slag to sub-ppm level and that led to the refinement of the result and thus, better comparison. A very small temperature dependence of the concentration of precious metals was found with silver being an exception, whose solubility was inversely proportional with copper concentration in the matte. The solubility of PGEs in the silica-saturated iron silicate slag is lower than that of gold over entire concentration range. The distribution of silver is favorable towards the matte phase when the oxygen pressure of the matte-slag-gas system is higher and the same is also favored for a low-temperature process. Other precious metals showed an increasing trend as function of the matte grade. The distribution coefficients of precious metals such as Au, Pd, Pt and Rh were 1500, 3000, 6000 and 10000 respectively for matte grade of 65% Cu, while the same for Ag varied between 100–200 in the matte grade of 50–70% Cu. It was concluded that the distribution of precious metals in the matte and the slag phase was a function of the properties of the former.

The capabilities of LA-ICPMS was also profoundly exploited in the field of geology as well. Gilbert *et al.* studied five reference materials (8b, PGE-A, NiS-3, Po727-T1 and Po724-T) and the Lombard meteorite for determination of PGE and gold in order to assess the homogeneity of the materials and for comparison of consistency in calibration process[111]. The following isotopes viz., ^{57}Fe, ^{59}Co, ^{60}Ni, ^{65}Cu, ^{66}Zn, ^{99}Ru, ^{101}Ru, ^{103}Rh, ^{105}Pd, ^{106}Pd, ^{111}Cd, ^{189}Os, ^{193}Ir, ^{195}Pt and ^{197}Au were measured in time-resolved mode. A dwell time of 20 ms per isotope was used, resulting in a total sweep time of 0.31 s. Factors like ablation cell design, interface between laser probe and ICPMS a laser wavelength, may result in signal instability and hence signal uncertainty. Homogeneous distribution of elements was found for Po724-T, Po727-T1 and the Lombard meteorite, while persistent heterogeneity existed in terms of some elements in other RMs such as Pd in NiS-3 and Os in 8b. Osmium, Ir and Pd in PGE-A, Rh, Pt and Au in NiS-3 and Ir and Ru in 8b, albeit to different degrees. The NiS-3 was used to calibrate the LA-ICPMS instruments for other RMs. RMs 8b and Po727-T1 gave the most consistent results with measurement of the elements being same within 5%. The highest uncertainty was exhibited by Pd in the RMs, thus making a direct comparison of the RMs difficult. Gauert *et al.* reported on the analysis and comparison of various non-destructive techniques such as EPMA, XRF and LA-ICPMS for the trace element analysis in gold samples of gold deposits in South Africa[112]. A solid-state Nd:YAG laser operating at 213 nm was used for LA-ICPMS measurement avoiding any sample digestion procedures and lengthy process. The compositional overlap of the techniques was rather poor, with different techniques exhibiting preferential precision for only certain elements. While LA-ICPMS exhibited a strong scatter for Fe, Ni and Cu (especially for Fe probably due to presence of pyrite inclusion), EPMA showed large range of values for same sample for Fe and Ni, and precise value of Cu. While EPMA gave moderate to very good detection limit of ppm range and reproducible results, it requires smaller diameter thus ensuring sample of very small grain analysis. However, the trace element analysis, which sometimes requires techniques ensuring sub-ppb range LOD, cannot be done by EPMA independently. SR-μ-XRF also ensured reproducible results albeit with a detection limit that is intermediate to EPMA and LA-ICPMS. However, certain trace elements such as Cu, Zn, Ta, Zr and Nb suffers from the problem of line overlap (of

these elements) with that of Ag and Au for XRF with energies of 33.2 keV and above. LA-ICPMS has the lowest detection limit among the three but results are less reproducible and technique requires bigger grain for the scan and may indicate anomalous conclusion where inclusions are predominant e.g. pyrite inclusions. Zelenski *et al*. studied the composition of the early sulphide melts of the Tolbachik volcano, which might delineate the formation of magmatic sulphide ore deposits, in terms of PGE and Au by LA-ICPMS and electron microscopy[113]. Nineteen sulphide globules in olivine were investigated with LA-ICPMS for the distribution and concentration of elements such as PGE, Au and Re (siderophiles), Te (metalloid) and Zn, Ag, Cd, Pb and Bi (chalcophile), apart from major elements like Fe, Ni, Co, Cu and S. Trace elements including the precious metals were found to exist in the solid solution in sulphide phase in the bulk and phase boundaries in the form of nuggets. The highest concentration found in the globule for Au, Pd and Pt were 13.3, 299 and 115 ppm, respectively. A 193 nm Ar-F excimer laser was used with a beam size of 50 μm for the laser ablation purpose. Corrections were made on ^{106}Pd for isobaric interference for ^{106}Cd, accomplished by detecting the signal of ^{111}Cd. PGE-rich phases might also be the result of the formation of polyatomic metallic cluster, which agglomerates to form PGE phase. The precious metal accumulation in sulphide melts is a result of diffusive transport of metals from cogenetic silicate melts. However, some amount of PGE might also have been present in the silicate matrices which facilitated the nucleation of the PGEs. The cooling of the sulphide melts also resulted in the exsolvation of PGE-Au nuggets.

4.3. Neutron activation analysis

Instrumental neutron activation analysis has been a seeded technique in this respect and apart from precious metal other metals have also been precisely analyzed with this method[114–117]. It is based on the principle of bombardment of the object by an incident beam and subsequent measurement of the delayed emission of γ-radiation from nuclide. It is a non-destructive and multi-element analysis technique where sample is not supposed to be physically decomposed or chemically degraded. Many a times this technique has been combined with some other methods such as XRD/XRF to obtain precise results.

Guerra *et al*. reported on the study of gold by radiophysical methods such as neutron activation analysis/proton activation analysis[118]. Certain trace element like platinum, antimony, tin, palladium, etc. can be used to follow gold in ores/objects. Elements such as Ag, Au, Pd and Pt among many others were determined by activation analysis, mainly in coin samples. Activation analysis has been compared with other techniques like particle induced X-ray emission (PIXE), particle induced γ-ray emission (PIGE) and laser ablation ICPMS as non-destructive methods to detect major and trace elements. It was found that PIGE gave a bad detection limit in nugget gold samples and could only be used complementary to PIXE. Heterogeneity of the samples had an effect on the PIXE analysis results mainly for major elements. Although proton activation analysis (PAA), fast neutron activation analysis (FNAA) and PIGE produced reliable results, but FNAA was time-consuming, comparatively expensive and could not be performed on large samples and very small samples could not be analyzed with PAA. Additionally, LA-ICPMS could not give quantitative results for representation of the complete sample. Sekimoto *et al*. reported on elemental analysis of few microgram of samples (meteoritic grain; chunk of Kilabo chondrite and magnetic spherule from Pacific ocean sea sediment) and compared the results with two reference samples viz., Allende meteoritic powder and basaltic rock reference sample prepared by Geological Survey of Japan[117]. The technique could detect gold in the Kilabo sample down to sub-pg level. INAA with more than 28 h irradiation under 5 MW operation was required for determination of gold (same for Sc, Zn, Ir).

NAA was carried out for dross samples from Government of India mint, Mumbai for quantitative determination of Ag and Ag[119]. The dross which may contain precious metals like Ag and Au apart from complex refractory material demands a technique (like NAA) which can analyze the elements in solid state as its dissolution would be very complicated. The method gave result compared to an internal monostandard (Na). The determination of gold was performed in different amount (less than 1 g to about 100 g) of sample quantity producing reliable results.

The method of activation analysis works very well for biomaterials such as bones where variation in the level of trace metals has a profound effect on bone metabolism leading to diseases like osteoporosis. Several studies in this line

have been performed on non-intact and intact bones without subjecting them to any pre-treatment, ashing or acid-digestion wherein some trace metal may be lost in the process. Zaichick *et al*. studied the effect of age and bone diseases on the variation of concentration of about 31 trace elements in rib bone of 24 healthy persons in the 16–55 year old age band by INAA[120]. Trace element data in CRM IAEA H-5 animal bone and SRM NIST 1486 bone meal found by INAA were used for comparison. The content of the trace elements including Ag and Au in all the samples were found to be below the detection limit. The same group applied NAA in the study of 38 trace elements including Ag and Au in human femoral neck of 85 healthy individual[121] and studied the effect of age in intact human prostrate[122].

While assessing such waste products with heat and acid treatments is a cumbersome job, their analysis with non-destructive techniques like NAA offers a vast scope. Tickner *et al.* reported on determination bulk amount of electronic and automotive waste materials for recyclable, precious and hazardous elements with NAA[123]. The content of valuable elements such as silver and gold is found to vary 250–350 ppm and 80–800 ppm in electronic waste respectively, while the automotive waste does not contain such element in detectable amount. Palladium was also found to have considerable contribution in such wastes. The adopted method was found to be rapid without any requirement of sample preparation time and results were obtained within few minutes confirming the broad scope of its application in larger scale in near future.

4.4. LIBS

LIBS is a modern technique for qualitative and quantitative detection of a large spectrum of chemical species in a variety of samples requiring minimum pretreatment or sample preparation. The method involves bombardment of a the sample with a pulsed laser beam (generally Nd:YAG laser) for a short duration (few nanoseconds) focused on a small area and the subsequent emission of radiation, which is characteristic of every element. The laser induces ablation of the target material and production of plasma. The plasma emission produces two kinds of radiation, viz., a broad continuum radiation and discrete radiation lines. The excited species emit radiation at different wavelengths which as characteristic of the element/species and thus allowing their identification. Quantitative determination of the elements is possible by the measurement of the intensity of the emitted lines. This is an attractive technique for geochemical and environmental application[124–127].

With the emerging application of precious metals in various industrial application, certain fast and accurate non-destructive analytical technique like LIBS becomes quintessential. For example, in automobile industry, where the application of expensive metals such as PGM especially Pd and Pt is very frequent in automobile catalyst, LIBS has the potential to play a crucial role in analysis and recycling processes. Asimellis *et al*. reported on the application of LIBS for analysis of automobile catalyst slurry for recycling process of PGMs[128]. Fast spectroscopic analysis (1.5 min/sample) was designed on the basis of linear best-fit calibration curves and with the proper selection of interference-free spectral lines which resulted in very accurate and precise measurements in the range of 5 wt.% to few ppm. For Pd, spectral line at 340.46 nm exhibit minimum interference while for Pt, a broad range of interference-free lines was screened viz. 270.24, 270.59, 271.90 and 273.39 nm. Legnaioli *et al*. demonstrated the application of LIBS as a promising competitor to complicated and expensive techniques like ICPOES and XRF for evaluation and recycling of precious metals from industrial waste materials such as catalysts, batteries, electronic circuit boards, electronic gadgets, etc.[129]. The technique was cautiously modified to minimize the effect of self-absorption effect of emission lines for Ag and Au considering a higher dilution factor, and choosing the maximum intensity spectral lines at 338.3 nm and 267.6 nm respectively. It is worthy to mention that the calibration curves for Ag and Au were non-linear owing to the aforementioned phenomenon. The spectral line chosen for Pt i.e. 306.5 nm suffered a spectral interference from Cu line (306.3 nm) resulting in an imperfect calibration curve with a non-zero intercept. The results obtained were compared with XRF data for direct evaluation. In a modified technique, Lou *et al.* explained the difference and advantage of a double-pulse LIBS technique for the determination of silver jewelry compared to the single-pulse one[130]. It was concluded that the merit of double-pulse LIBS included very high signal enhancement and low energy consumption. Ahmed *et al*. applied LIBS in combination with LA-TOF-MS to determine the purity of gold alloy cartage, with a low limit of detection for Au (0.05 ppm) and extended its ap-

plicability to gold ornaments without any sample preparation[131].

LIBS also did not lag behind in the analysis of living biological materials. For instance, Galiová *et al.* demonstrated the study of the spatial distribution of Ag and Cu achieved by the technique of LIBS and LA-ICPMS *Helianthus annuus* L. plant samples[132]. The self-absorption effect was studied by choosing two spectral lines for Ag viz. 328.07 nm and 338.29 nm with different transition probability (4 and 2 respectively). The ratio of the intensity of two lines would be ideally (in the absence of self-absorption) in the ratio 2:1. The measurement conditions were optimized to achieve minimum self-absorption effect. It was found that Ag concentrated more in the central vein while Cu distributed more uniformly across the samples.

One of the most widespread use of LIBS lies in the study of variety of archaeological samples and thus extensive study have been attempted with the use of this technique. Pardini *et al.* studied the Roman silver denarii with the help of LIBS and XRF and elucidated on its composition and metallurgy of the period[133]. Comparative data of Ag and Cu helped in explaining the different information of Roman history. The study aids a lot in the authentication and dating of the archaeological artefacts like coins. Ahmed *et al*. analyzed the samples of historical Egyptian textile samples for various elements by LIBS and SEM-EDS methods[134]. The main elements as found by LIBS were Cu, Ag and Au among other minor trace amounts of Al, Ca, Na and Mg. It is found that the textile fibre mainly composed of the Cu-Ag-Au alloy and the trace amount of other elements were probably due to corrosion and handling. This confirmed the unsuitable environment and improper handling and storage of these materials. The LIBS data were corroborated by SEM-EDS method and the former has a promise for fast non-destructive analysis of such samples.

4.5. Other miscellaneous techniques

The evolution of different allied and complementary techniques such as SEM-EDS, FT-IR, TEM, SIMS, XPS, EPMA, EBSD, Raman and its variants, have led to the critical observation of minute details and consequent explanation of solid sample/substance/materials. Most of the time, these methods have been used in combination to each other and/or other analytical techniques for complete analysis of the materials since the sample under analysis cannot be destroyed and handled carefully. Samples from various backgrounds such as industrial, geological, archaeological, etc. have been addressed.

Archaeological samples have long been a hot object of study using the aforementioned techniques since their preservation is quintessential. Guerra *et al.* analyzed ancient gold works (jewelry and coinages) with non-destructive techniques such as SEM-EDS, portable XRF and PIXE in order to determine its structural features and chemical nature[135]. SEM-EDS gives information about the structure and elemental analysis and XRF and PIXE gave composition of the material employed. PIXE analysis of one of the Etruscan Helios' head from the Campana's collection (4th-3rd century BC) shows that the concentration of gold alloy in the ancient part and the modern wires were 2.1±0.1% Ag and 0.7±0.1% Cu, and 7.9±0.2% Ag and 1.6±0.3% Cu, respectively. Louviers ring bezel (Merovingian jewellery) contained PGE inclusion with varying diameter (10–150 μm). Ir, Os and Ru (the biggest inclusion consisting of 57% Ir, 37% Os, 6% Ru) were confirmed by SEM-EDS and PIXE data. The Sn content of the gold artefacts also confirms their origin (some cases being same; the Roman coins analyzed all had Sn below 230 ppm). Weiszburg *et al.* made a detailed study of the gilt silver/gold works in historical textile samples (sampled without deforming/destroying them using focussed ion beam milling) of Medieval and post-Medieval period in European provenances, with the application of HR-SEM, TEM-EDS, EPMA, EBSD, and micro-Raman techniques[136]. The study was done to understand the objects in term of its structure, morphology and composition. Phase determination and copper inclusion in the gilts were done by TEM. Two types of silver base could be distinguished: one with low copper content (0.5–2.5 wt%) in wires and two-sided strip gilt and other high copper (4–10 wt%) one-sided strip gilt, incorporating heterogeneous distribution of two generations of copper phases in the latter high concentration gilt. Silver was found to include copper in solid solution in wire samples. A paramelaconite type (Cu_4O_3) micro-Raman spectra was observed (I-type) with the angular or isometric inclusion of copper and oxygen (but no carbon or sulphur). Textural inhomogeneity was prevalent in the samples (20–400 nm). SEM was used to study the microstructure, EBSD and TEM to study the crystal phases, EPMA for elemental analysis and micro-Raman spectroscopy was applied for inclusion of silver base. Gold

coatings were visible from SEM images at the cross-sections. Diffusion bonding was present as evident form finger-like gold intrusions in silver base. Absence of foreign metal inclusions in the gold-silver interface discards the use of fire-gilding method. Selective corrosion due to local galvanic attack was also visible. The use of any single technique in the study of these artefacts may be misleading owing to the inherent in homogeneity and internal corrosions suffered by the age-old object and thus a combination of various reliable methods is necessary to explain their features.

Righter *et al.* studied the abundance of highly siderophile elements in the interior of Mars (mantle) where core formation takes place at very high temperature and pressure (around 14 GPa and 2000°C)[137]. The study of the elements mentioned above paves the way for understanding the accretion process owing to the strong affinity of the elements for FeNi and sulphides. Metal-silicate partitioning data for PGEs and Au and Re are reported. The adopted model calculation takes into account various processes such as malting, fractional crystallization and sulphide saturation in understanding the Martian geology. ICPMS, TEM and SIMS data were combined to obtain detailed information about the elemental distribution. One such condition reports the following composition of mantle (with their D metal/silicate values): Au = 0.63 ppb (1000), Pd = 4.22 ppb (600), Pt = 4.98 ppb (900), Re = 0.05 ppb (3200), Ru = 1.8 ppb (1800), Os = 1.8 ppb (1000), and Ir = 2.2 ppb (1000) (Fig. 6; Table 4) [D is the partition coefficient]. Reith *et al*. investigated a very interesting process of the contribution of biological factors in formation/transformation of mineral grains or nuggets in PGEs[138]. SIMS and LA-ICPMS were applied to study the composition of the obtained geological materials. PGM grains were collected from different sites like Brazil, Columbia and Australia. About 20 Pt-Pd grains (0.2–3.0 mm size) were collected from sediments at CorregoBomSucessoGarimpo, Brazil. Bacterial cells and exopolymeric substances were found on the surface of the grains suggesting a biogeochemical process of their formation. Presence of biophilic elements such as C, N, S, Se and I (from SIMS data), inside the metallic Pt-Pd matrix also affirms a biological process. Bacterial community associated with the Pt-Pd grains of Brazil were chiefly responsible for biomineralization. For example, C. metallidurans, a β-proteobacterium, absorbs Pt(IV) ions from solutions (in extracellular substances c.f. Au mineralization which takes place in cytoplasm) and converts them into Pt nanoparticles as suggested by experiments. The above study confirms the bacterial role in (*trans*)formation of PGE grains and the underlying process in dispersion and re-concentration in surface environment.

Recently, Sen Gupta *et al.* applied SIMS analysis in the study of uptake of noble metal (Ag) in cereal plants (rice)[139]. Various factors like environment, soil composition, rice variety and site of metal accumulation were studied in details. SIMS, XPS, SEM-EDS and ICPMS method were adopted for various analyses. It was found that the metal concentrates mostly in the grains and lowest in the leaves. Among 505 rice varieties studied, Garib-sal (from West Bengal, India) showed considerably high concentration in the grains (15.61 ppm), followed by Kharah (5.60 ppm) and Subasita (4.70 ppm). Bioaccumulation of silver in Garib-sal variety was around 100 times more than other normal cultivars. The crops when grown in a soil enriched with Ag^+ ions (from $AgNO_3$ solution) showed a steep rise in Ag uptake by the plants. EDS and XPS were unable to detect Ag in the plant due to their high detection limit. The microstructure of the grains remains unchanged as suggested by SEM. Finally, NanoSIMS data was used in the mapping of Ag in the grains; Ag peak at 107 amu was used as the peak at 109 encounters more interferences. NanoSIMS data also showed heterogeneous distribution of ^{107}Ag in the grains. While the concentration of Ag decreased gradually from aleurone to subaleurone layer of rice bran, a negligible concentration of Ag was found in the interior part of endosperm. Due to its antimicrobial property, Ag-fortified rice grain can cure GI microbial infection.

Simon *et al.* synthesized and studied a composite material comprising of a precious metal (Ag NPs) dispersed on ZnO layers (Ag/ZnO system) and studied their morphological and compositional features with SEM-EDS, STEM, GIXRD and XPS[140]. XPS has been thoroughly exploited to investigate the systems involving thin (metal/metal oxide) and metallic NPs[141–143]. In the reported work, Ag NPs were dispersed by sputtering method onto ZnO layers deposited with PECVD in order to tailor the physical aspects of the composite system such as orientation and composition. This system was further employed in production and sensing of H_2 gas by

photo-assisted transformation of alcoholic solution. Ag NPs were obtained in the size range of 5–20 nm. XPS confirmed the surface chemical composition of the composite system. It was found that thermal treatment lead to decrease in Ag content due to aggregate formation and diffusion of the Ag in the ZnO layers which indicates proper post-annealing is required for sensing applications. Auger measurements (undertaken since the BE of Ag(0) and Ag(I) are very close) indicated that the main silver component in the as-prepared and annealed material were Ag(I) and Ag(0) respectively, suggesting a reduction process. An electronic interaction between Ag and ZnO was indicated by the increase of surface $Zn2P_{3/2}$ BEs with increase in Ag amount. The detailed analysis of the composite materials paves the way for further improvement and application of such systems for sensing and catalytic activities. Sutter *et al*. did some *in situ* and *ex situ* experiments on mechanism and other aspects of galvanic reactions of Ag NP and $[PdCl_4]^{2-}$ species in solution, which has potential for electrocatalyst in fuel cells, and monitored the same by TEM, XPS and liquid cell electron microscopy[144]. The galvanic replacement reaction between Ag NP and $[PdCl_4]^{2-}$ species were studied in presence and absence of high-energy electron radiation. These type of reactions produces hollow and porous noble metal nanostructures capable of acting as nanocages/nanoboxes (in biomedical applications), catalysts and optically active materials. With reaction time, as observed in absence of electron radiations, the hollow structures with increased size (36–44 nm) were produced with silver concentration in the range of 65–70%. The Ag $3d_{5/2}$ peaks (~368.15 eV) in the product material shifted to a lower BE compared to Ag NP (~368.3 eV) owing to the formation of Ag-Pd alloy as observed by XPS. Similar effect was not persistent in Pd peak due to the insensitivity of Pd on alloy formation (a minor shift of 0.1 eV). Pd content reach a maximum of 30–35% under adopted conditions. The real time measurements showed the presence of hydrated electrons which can react with metal ions/complexes to form hydroxyl radicals resulting in homogeneous nucleation of Pd on Ag NP and the available redox atmosphere (quenching of OH radical by alcohol) lead to the lower oxidation rate of Ag and higher reduction of $[PdCl_4]^{2-}$ and subsequent formation of Ag-Pd core-shell nanostructures. Meng *et al.* analyzed the Ag NP loaded graphene (also graphene oxide) prepared for tribological application as lubricating additive in engine oil and tested the same in four-ball tribometer[145]. The composite material was synthesized in supercritical CO_2 by a facile chemical reduction pathway. The synthesized material was analyzed with XPS, XRD, TGA and TEM. It was used as an additive in 10w40 engine oil, and is observed to exhibit friction-reducing and anti-wear characteristics. Several peaks of nano-Ag were observed in XRD for different planes viz. (111), (200), (220), (222), and (311), which are found to be broadened upon formation of the composite material due to the decrease in grain size. The different weight loss from room temperature to 600°C in TGA suggest different amount of Ag in Sc-Ag/GN and Ag/GN (Sc-CO2 lead to more efficient incorporation and transfer of Ag, from $AgNO_3$ into the graphene layer). XPS spectra gives a detailed picture of the nanocomposite. The diminished C/O atomic ratio in the Ag/GN and Sc-Ag/GN, compared to graphene oxide suggests the reduction of the latter. The C/O ratio was greater for Sc-Ag/GN compared to Ag/GN indicating that the reduction process was extensive in presence of Sc-CO2. Moreover, the difference in C1s spectra of Sc-Ag/GN and Ag/GN suggest their variable chemical composition. The spectra of Ag3d shows the presence of Ag(0) in silver NP of both Sc-Ag/GN and Ag/GN. The lubricating property of the composite material probably resulted from the synergistic interaction of Ag NP and graphene and has a promise for industrial application. Volkov *et al*. studied the different modes of interaction of metal Ag-DNA *in vacuo* and Ag^+-DNA and fluorescent DNA-Ag complexes in solution with the help of detailed XPS analysis[146]. Since silver is a bioactive element, its interaction with a living unit such as DNA is a matter of interest. Moreover, Ag forms fluorescent complexes with DNA that can be harnessed for flexible optoelectronics and organic phosphors. Therefore, the stability and binding property of the two must be investigated under different conditions. Here a powerful tool such as XPS has been applied to understand the state and binding of the elements of Ag-DNA compound and confirm the composition and oxidation state of the elements. The metallic Ag-DNA complex formed *in vacuo*, comprised of Ag binding mainly with oxygen atom of phosphodiester and deoxyribose of DNA. The core level O 1s spectrum, split into two peaks: one at 531.3 eV has been assigned to the C=O, P=O, and $P\text{-}O^-$ groups and the other at 532.8 eV, indicates C-O-C and C-O-P groups of DNA. The later peak may also be due to water adsorbed on graphite cleavage or DNA

Table 3. Comparison chart for non-destructive analytical techniques with respect to the nature of samples

Nature of sample	Ions analyzed	Detection range	Complementary technique(s)	Literature
XRF				
Geological ore samples, sulphide and chromite bearing reference materials	Au, Pd, Pt	Percentage level	EDS	103
Silver coins of Trajan (AD 98-117)	Ag	Percentage level	SEM/EDS	104
Municipal solid waste samples	Ag, Au, Pd, Pt and other non-precious elements	Percentage to ppm level	—	105
Electronic circuit boards	Ag, Au, and other non-precious elements	Percentage to ppm level	—	106
LA-ICPMS				
Celtic gold coins	Ag, Au, and other non-precious elements	Percentage to ppm level	EPMA	107
Muisca goldwork of Colombia	Cu, Ag, Au, PGE and other non-precious elements	Percentage level	pXRF	108
Industrial sample	Ag, Au, Pd, Pt and other non-precious elements	Percentage to ppm level	EPMA	110
Geological reference materials and Lombard meteorite	Au and PGE	Percentage to ppm level	—	111
Geological gold deposits of South Africa	Ag, Au, Pd, Pt and other non-precious elements	Percentage to ppm level	EPMA, XRF	112
Sulfide melts from modern arc basalt (Tolbachik volcano, Kamchatka)	Au and PGE	Percentage to ppm level	EDS	113
Neutron/Gamma activation analysis				
Gold alloy samples	Cu, Ag, Au	Percentage to ppm level	ICPMS, PIXE, PIGE	118
Meteoritic grains	Au and other non-precious elements	Sub-pg level	—	117
Dross samples from mint	Ag, Au	ppm level	—	119
Human bone samples	Ag, Au and other non-precious elements	ppm level	—	120
Femoral neck	Ag, Au and other non-precious elements	ppm level	—	121
Electronic waste	Ag, Au, Pd and other non-precious elements	ppm level	—	123
LIBS				
Automobile catalyst scrap	Pd, Pt, Rh	Percentage to ppm level	—	128
Industrial waste materials	Ag, Au, Pd, Pt, Rh	Sub-percentage to percentage level	XRF	129
Silver jewellery	Ag	Percentage level	—	130
Gold alloy samples and ornaments	Cu, Ag, Au	Percentage to ppm level	LA-TOF-MS	131
Biological sample	Cu, Ag	—	LA-ICPMS	132
Roman silver denarii	Cu,Ag	Percentage level	XRF	133
Ancient Egyptian textile specimen	Cu, Ag, Au and other non-precious elements	—	SEM-EDS	134
Miscellaneous techniques				
Ancient gold work	Cu, Ag, Au	Percentage level	SEM-EDS, portable XRF and PIXE	135

Table-3 (contd.)

Historical textile samples	Cu, Ag, Au	Percentage level	HR-SEM, TEM-EDS, EPMA, EBSD, and micro-Raman spectroscopy	136
Martian sample	Au, Re, PGEs and other non-precious elements	Percentage to ppm level	ICPMS, TEM-EDS, SIMS	137
Geological samples from Brazil, Australia and Columbia	Pd, Pt	Sub-percentage level	SIMS, LA-ICPMS, SEM	138
Rice plant samples	Ag	ppm level	SIMS, XPS, SEM-EDS and ICPMS	139
Nanocomposite material	Ag, Zn	—	SEM-EDS, STEM, GIXRD and XPS	140
Catalyst	Ag, Pd	—	TEM, XPS and liquid cell electron microscopy	144
Graphene-based lubricating additive	Ag	—	XPS, XRD, TGA and TEM	145
DNA samples	Ag	—	XPS	146

film. A redistribution of N 1s spectrum (resolved into two peaks) observed for DNA-Ag^+ system was clearly visible with the second component shifting to a lower BE side indicating an increase in electron density due to binding with Ag^+. The Ag^+ showed a preferential binding to N3 of cytosine, which is corroborated by the quantum mechanical calculation that indicate an enhanced negative charge on N3 of cytosine (in cytosine-Ag^+ species) compared to the free cytosine species. In the fluorescent Ag-DNA complex a slight increase in the BE of bound Ag (~0.2 eV) compared to Ag(0) NP was observed.

5. Summary and outlook

The inevitable versatility of the substances and materials have led to extensive use of different metals, which in turn generates huge amount of wastes containing the toxic lethal dose of the heavy and other metal ions causing ecological imbalance. These metallic ions are leached into the environment and ultimately reach the body. Therefore, multiple techniques were applied to detect them. While the delicate and historic archaeological objects were analyzed with non-destructive techniques so that they can be preserved unscathed with percentage to ppm level concentrations, the typical geological soil and rock materials were subjected to "harsh" acid-based digestion technique to extract the metal from silicate envelope and then analyzed for the elements with suitable spectroscopic or spectrometric techniques such as AAS or ICPMS taking their detection capacity to ppm and ppb level. In certain cases, where amount of analyte is very low, a preconcentration technique such as SPE is indelible and aids the analysis by enriching the metal in the analyte solution that is fed into the instrument. The non-destructive techniques elaborated with examples from different principles and different sample backgrounds duly summarize the requirement and suitability of the methods comparing the technology available. The complementary techniques that can be used to corroborate the results for quantification of the samples have been presented from recent literature. Moreover, when the instruments developed with modern technological thrust and become more complicated and expensive, another subtle solution is the use of chemosensors for determination of the metal in solution. These chemical substances changes color in the solution according to the amount of analyte and precisely detect the metal ion qualitatively and quantitatively in a comparatively less complicated manner. The chemosensors discussed in this article presents an overview of the nature and structure of compounds that can detect the precious metal ions and correlates the analyte ion with the chemical anatomy of the sensor that is necessary for the detection of particular ion with low limit of detection. It can be conclusively stated that the determination of precious metals in samples is intricately dependent on the origin of the sample, shape and texture, and concentration of the analyte in the sample, and therefore, no single instrument can be used for their determination.

Acknowledgement

The author is thankful to Geological Survey of India for giving permission to publish this work. Thanks are also due to Dr. V. K. Srivastava for the encouragement and support.

Abbreviations

AAS	Atomic Absorption Spectroscopy
amu	Atomic Mass Unit
BC	Before Christ
BE	Binding Energy
CNT	Carbon Nanotube
CRM	Certified Reference Material
CVAAS	Cold Vapor Atomic Absorption Spectroscopy
DMSO	Dimethyl Sulfoxide
DNA	Deoxyribonucleic Acid
EBSD	Electron Back-Scattered Diffraction
EDS	Energy-Dispersive X-ray Spectroscopy
EDTA	Ethylenediaminetetraacetic Acid
EPMA	Electron Probe Microanalyzer
ESI-MS	Electrospray Ionization Mass Spectrometry
ETAAS	Electrothermal Atomic Absorption Spectroscopy
FAAS	Flame Atomic Absorption Spectroscopy
FNAA	Fast Neutron Activation Analsyis
FRET	Fluorescence Resonance Energy Transfer
FT-IR	Fourier Transform Infrared Spectroscopy
GFAAS	Graphite Furnace Atomic Absorption Spectroscopy
GIXRD	Grazing Incidence X-ray Diffraction
HGAAS	Hydride Generation Atomic Absorption Spectroscopy
HPLC	High Performance Liquid Chromatography
HR-SEM	High Resolution Scanning Electron Microscopy
ICPAES	Inductively Coupled Plasma Atomic Emission Spectroscopy
ICPMS	Inductively Coupled Plasma Mass Spectrometry
ICPOES	Inductively Coupled Plasma Optical Emission Spectroscopy
INAA	Instrumental Neutron Activation Energy
LA-ICPMS	Laser Ablation Inductively Coupled Plasma Mass Spectrometry
LA-TOF-MS	Laser Ablation Time-Of-Flight Mass Spectrometry
LOD	Limit Of Detection
LOQ	Limit Of Quantification
MOF	Metal Organic Framework
MWCNT	Multi-Walled Carbon Nanotube
NAA	Neutron Activation Analysis
NMR	Nuclear Magnetic Resonance
NP	Nano Particle
PAA	Proton Activation Analysis
PECVD	Plasma Enhanced Chemical Vapor Deposition
PET	Photoinduced Electron Transfer
PGE	Platinum Group Elements
PIGE	Proton Induced Gamma Emission
PIXE	Proton Induced X-Ray Emission
ppb	Parts Per Billion
ppm	Parts Per Million
ppt	Parts Per Trillion
pXRF	Portable X-ray Fluorescence
QD	Quantum Dot
RM	Reference Material
SEM	Scanning Electron Microscopy
SIMS	Secondary Ion Mass Spectrometry
SPE	Solid Phase Extraction
SR-μ-XRF	Synchrotron Radiation Micro-X-ray Fluorescence
STEM	Scanning Tunnelling Electron Microscopy
TGA	Thermogravimetric Analysis
TEM	Transmission Electron Microscopy
TMK	Thiomichler's Ketone
UV	Ultraviolet
VSM	Vibrating Sample Magnetometer
XPS	X-ray Photoelectron Spectroscopy
XRD	X-ray Diffraction
XRF	X-ray Fluorescence
YAG	Yttrium Aluminum Garnet

References

1. D. Astruc and M.-C. Daniel, *Chem. Rev.,* 2004, **104**, 293.
2. C. M. Cobley, J. Chen, E. C. Cho, L. V. Wang and Y. Xia, *Chem. Soc. Rev.,* 2011, **40**, 44.
3. T. K. Sau and A. L. Rogach, *Adv. Mater*., 2010, **22**, 1781.
4. A. R. Tao, J. Huang and P. Yang, *Acc. Chem. Res.,* 2008, **41**, 1662.
5. A. R. Tao, S. Habas and P. Yang, *Small*, 2008, **4**, 310.
6. J. Chen, B. Lim, E. Lee and Y. Xia, *Nano Today*, 2009, **4**, 81.
7. S. E. Skrabalak, J. Chen, Y. Sun, X. Lu, L. Au, C. M. Cobley and Y. Xia, *Acc. Chem. Res*., 2008, **41**, 1587.
8. B. Wiley, Y. Sun and Y. Xia, *Acc. Chem. Res*., 2007, **40**, 1067.
9. S. R. Taylor, *Geochim. Cosmochim. Acta*, 1964, **28**, 1273.
10. L. Tan and Y. Chi-lung, *Int. Geol. Rev*., 1970, **12**, 778.
11. A. B. G. Lansdown, Silver in Health Care: Antimicrobial Effects and Safety in Use, in: Biofunctional Textiles and the Skin, Basel, KARGER, 2006, 17.
12. A. B. G. Lansdown, *Adv. Pharmacol. Sci*., 2010, **2010**, 1.
13. X. Huang, Y. Wang, X. Liao and B. Shi, *J. Hazard. Mater*.,

2010, **183**, 793.

14. K. E. Jarvis, S. J. Parry and J. M. Piper, *Environ. Sci. Technol.*, 2001, **35**, 1031.
15. J. Kielhorn, C. Melber, D. Keller and I. Mangelsdorf, *Int. J. Hyg. Environ. Health*, 2002, **205**, 417.
16. B. C. Hagelüken, *Platin. Met. Rev.*, 2012, **56**, 29.
17. World Health Organization, Environmental Health Criteria 125-Platinum, World Health Organization, International Programme on Chemical Safety, Geneva, 1991.
18. T. Gebel, Toxicology of platinum, palladium, rhodium, and their compounds, in: Zereini F., Alt F. (eds) Anthropogenic Platinum-Group Element Emissions, Springer, Berlin, Heidelberg, 2000.
19. J. Pawlak, E. £odyga-Chruœciñska and J. Chrustowicz, *J. Trace Elem. Med. Biol.*, 2014, **28**, 247.
20. S. Cerovac, V. Guzsvány, Z. Kónya, A. M. Ashrafi, I. Švancara, S. Ronèeviæ, A. Kukovecz, B. Dalmacija and K. Vytøas, *Talanta,* 2015, **134**, 640.
21. M. Kaykhaii and S. Noorinejad, *J. Anal. At. Spectrom.*, 2014, **29**, 875.
22. M. Banerjee, V.-S. Dang, M. Bledowski, R. Beranek, H.-W. Becker, D. Rogalla, E. Edengeiser, M. Havenick, A. Wieck and A. Devi, *Chem. Vap. Depos.*, 2014, **20**, 224.
23. P. Wang, K. Jiang, G. Wang, J. Yao and X. Huang, *Angew. Chemie Int. Ed.*, 2016, **55**, 12859.
24. I. A. Okorie, J. Enwistle and J. R. Dean, *Curr. Sci.*, 2015, **109**, 938.
25. M. H. Mashhadizadeh, M. Amoli-Diva, M. R. Shapouri and H. Afruzi, *Food Chem.*, 2014, **151**, 300.
26. J. Scheer, S. Findenig, W. Goessler, K. A. Francesconi, B. Howard, J. G. Umans, J. Pollak, M. Tellez-Plaza, E. K. Silbergeld, E. Guallar and A. Navas-Acien, *Anal. Methods*, 2012, **4**, 406.
27. J. Wan, K. Zhang, C. Li, Y. Li, and S. Niu, *Sensors Actuators, B: Chem.*, 2017, **246**, 696.
28. P. Petrova, S. Velichkov, N. Velitchkova, I. Havezov and N. Daskalova, *Spectrochim. Acta, Part B, At. Spectrosc.*, 2010, **65**, 130.
29. N. Ozturk, V. N. Bulut, C. Duran and M. Soylak, *Desalination*, 2011, **270**, 130.
30. I. De La Calle, N. Cabaleiro, M. Costas, F. Pena, S. Gil, I. Lavilla and C. Bendicho, *Microchem. J.*, 2011, **97**, 93.
31. W.-H. Hsu, S.-J. Jiang and A. C. Sahayam, *Anal. Chim. Acta*, 2013, **794**, 15.
32. H. Matusiewicz and M. Œlachciñski, *J. Anal. At. Spectrom.*, 2010, **25**, 1324.
33. V. Balaram, D. Vummiti, P. Roy, C.Taylor, P. Kar, A.K. Raju and K. Abburi, *Curr. Sci.*, 2013, **104**, 1207.
34. R. R. Barefoot, *J. Anal. At. Spectrom.*, 1998, **13**, 1077.
35. G. S. Reddi and C. R. M. Rao, *Analyst*, 1999, **124**, 1531.
36. L. Balcaen, E. Bolea-Fernandez, M. Resano and F. Vanhaecke, *Anal. Chim. Acta*, 2015, **894**, 7.
37. A. Akcil, C. Erust, C. S. Gahan, M. Ozgun, M. Sahin and A. Tuncuk, *Waste Manag.*, 2015, **45**, 258.
38. J. Hassan, N. Zari, K. Tabar-Heydar and S. H. Ahmadi, *J. Anal. Sci. Technol.*, 2016, **7**, 22.
39. T. Suoranta, M. Niemelä and P. Perämäki, *Anal. Methods,* 2014, **6**, 9321.
40. M. Karimi, V. Amani, F. Aboufazeli, H. Reza Lotfi Zadeh Zhad, O. Sadeghi and E. Najafi, *J. Chem.*, 2013, **2013**, 1.
41. X. Jin and H. Zhu, *J. Anal. At. Spectrom.*, 2000, **15**, 747.
42. P. Halli, J. J. Heikkinen, H. Elomaa, B. P. Wilson, V. Jokinen, K. Yliniemi, S. Franssila and M. Lundström, *ACS Sustainable Chem. Eng.*, 2018, **6**, 14631.
43. M. Tuzen, K. O. Saygi and M. Soylak, *J. Hazard. Mater.*, 2008, **156**, 591.
44. E. Mladenova, I. Dakova, I. Karadjova and M. Karadjov, *Microchem. J.*, 2012, **101**, 59.
45. M. Behbahani, F. Najafi, M. M. Amini, O. Sadeghi, A. Bagheri and P. G. Hassanlou, *J. Ind. Eng. Chem.*, 2014, **20**, 2248.
46. M. R. Awual and M. Ismael, *Sensors Actuators, B: Chem.*, 2014, **196**, 457.
47. Z. Tu, S. Lu, X. Chang, Z. Li, Z. Hu, L. Zhang and H. Tian, *Microchim. Acta*, 2011, **173**, 231.
48. E. Kazemi, S. Dadfarnia and A. M. Haji Shabani, *Talanta*, 2015, **141**, 273.
49. F. H. Moghaddam, M. A. Taher, M. Behzadi and M. Naghizadeh, *Microchim. Acta*, 2015, **182**, 2123.
50. M. Behbahani, T. Gorji, M. Mahyari, M. Salarian, A. Bagheri and A. Shaabani, *Food Anal. Methods*, 2014, **7**, 957.
51. N. Jalilian, H. Ebrahimzadeh, A. A. Asgharinezhad and K. Molaei, *Microchim. Acta*, 2017, **184**, 2191.
52. M. H. Yap, K. L. Fow and G. H. Chen, *Green Energy & Environment*, 2017, **2**, 218.
53. A. Bagheri, M. Taghizadeh, M. Behbahani, A. A. Asgharinezhad, M. Salarian, A. M. Dehghani, H. Ebrahimzadeh and M. M. Amini, *Talanta*, 2012, **99**, 132.
54. B. Volesky, *Trends Biotechnol.*, 1987, **5**, 96.
55. S. W. Won, P. Kotte, W. Wei, A. Lim and Y.-S. Yun, *Bioresour. Technol.*, 2014, **160**, 203.
56. X. Ju, K. Igarashi, S. Miyashita, H. Mitsuhashi, K. Inagaki, S. Fujji, H. Sawada, T. Kuwabara and A. Minoda, *Bioresour. Technol.*, 2016, **211**, 759.
57. V. N. Losev, O. V. Buyko, E. V. Borodina, A. S. Samoilo, A. M. Zhyzhaev and B. A. Velichko, *SeSci. Technol.*, 2018, **53**, 1654.
58. M. Dong, Y. W. Wang and Y. Peng, *Org. Lett.*, 2010, **12**, 5310.
59. A. Shahat and S. Trupp, *Sensors Actuators, B: Chem.*, 2017, **245**, 789.

60. J. F. Zhang, Y. Zhou, J. Yoon and J. S. Kim, *Chem. Soc. Rev*., 2011, **40**, 3416.
61. Z. Xu, S. Zheng, J. Yoon and D. R. Spring, *Analyst*, 2010, **135**, 2554.
62. T. Chen, W. Zhu, Y. Xu, S. Zhang, X. Zhang and X. Qian, *Dalton Trans*., 2010, **39**, 1316.
63. A. D. Arulraj, R. Devasenathipathy, S. M. Chen, V. S. Vasantha and S. F. Wang, *Sens. Bio-Sensing Res*., 2015, **6**, 19.
64. V. Tharmaraj, S. Devi and K. Pitchumani, *Analyst*, 2012, **137**, 5320.
65. M. Schmittel and H. Lin, *Inorg. Chem*., 2007, **46**, 9139.
66. H. Lin, M. E. Cinar and M. Schmittel, *Dalton Trans*., 2010, **39**, 5130.
67. J. S. Kim, O. J. Shon, J. A. Rim, S. K. Kim and J. Yoon, *J. Org. Chem*., 2002, **67**, 2348.
68. J. S. Kim, K. H. Noh, S. H. Lee, S. K. Kim, S. K. Kim and J. Yoon, *J. Org. Chem*., 2003, **68**, 597.
69. S. Huang, S. He, Y. Lu, F. Wei, X. Zeng and L. Zhao, *Chem. Commun*., 2011, **47**, 2408.
70. M. Kandaz, O. Güney and F. B. Senkal, *Polyhedron*, 2009, **28**, 3110.
71. N. Iki, M. Ohta, T. Tanaka, T. Horiuchi and H. Hoshino, *New J. Chem*., 2009, **33**, 23.
72. C.-Y. Lin, C.-J. Yu, Y.-H. Lin and W.-L. Tseng, *Anal. Chem*., 2010, **82**, 6830.
73. Y.-W. Wang, M. Wang, L. Wang, H. Xu, S. Tang, H.-H. Yang, L. Zhang and H. Song, *Sensors*, 2017, **17**, 2521.
74. A. Selva Sharma, T. SasiKumar and M. Ilanchelian, *J. Clust. Sci.,* 2018, **29**, 655.
75. X. E. Zhao, C. Lei, Y. Gao, H. Gao, S. Zhu, X. Yang, J. You and H. Wang, *Sensors Actuators, B: Chem*., 2017, **253**, 239.
76. T. Gong, J. Liu, X. Liu, J. Liu, J. Xiang and Y. Wu, *Food Chem*., 2016, **213**, 306.
77. T. G. Drummond, M. G. Hill and J. K. Barton, *Nat. Biotechnol*., 2003, **21**, 1192.
78. K. S. Park, J. Y. Lee and H. G. Park, *Chem. Commun*., 2012, **48**, 4549.
79. P. Miao, K. Han, B. Wang, G. Luo, P. Wang, M. Chen and Y. Tang, *Sci. Rep*., 2015, **5**, 1.
80. Y. Wu and R. Y. Lai, *Biotechnol. J*., 2016, **11**, 788.
81. A. Affrose, S. D. S. Parveen, B. S. Kumar and K. Pitchumani, *Sensors Actuators, B: Chem*., 2015, **206**, 170.
82. M. J. Jou, K. M. K. Swamy, H. N. Kim, H.-J. Kim, S.-G. Lee and J. Yoon, *Chem. Commun*., 2009, **46**, 7218.
83. O. A. Egorova, H. Seo, A. Chatterjee and K. H. Ahn, *Org. Lett*., 2010, **12**, 401.
84. Y.-K. Yang, S. Lee and J. Tae, *Org. Lett*., 2009, **11**, 5610.
85. J. H. Do, H. N. Kim, J. Yoon, J. S. Kim and H.-J. Kim, *Org. Lett*., 2010, **12**, 932.
86. M. Dong, Y.-W. Wang and Y. Peng, *Org. Lett*., 2010, **12**, 5310.
87. N. T. Patil, V. S. Shinde, M. S. Thakare, P. Hemant Kumar, P. R. Bangal, A. K. Barui and C. R. Patra, *Chem. Commun*., 2012, **48**, 11229.
88. J. E. Park, M. G. Choi and S. K. Chang, *Inorg. Chem*., 2012, **51**, 2880.
89. Y. Yang, C. Yin, F. Huo and J. Chao, *RSC Adv*., 2013, **3**, 9637.
90. E. A. Elshehy, S. A. El-Safty, M. A. Shenashen and M. Khairy, *Sensors Actuators, B: Chem*., 2014, **203**, 363.
91. A. Zuber, M. Purdey, E. Schartner, C. Forbes, B. van der Hoek, D. Giles, A. Abell, T. Monro and H. Ebendorf-Heidepriem, *Sensors Actuators, B: Chem*., 2016, **227**, 117.
92. A. Shahat and S. Trupp, *Sensors Actuators, B: Chem*., 2017, **245**, 789.
93. A. L. Garner, F. Song and K. Koide, *J. Am. Chem. Soc*., 2009, **131**, 5163.
94. M. E. Jun and K. H. Ahn, *Org. Lett*., 2010, **12**, 2790.
95. A. L. Garner and K. Koide, *J. Am. Chem. Soc*., 2008, **130**, 16472.
96. H. Li, J. Fan, F. Song, H. Zhu, J. Du, S. Sun and X. Peng, *Chem-A Eur. J*., 2010, **16**, 12349.
97. B. Liu, Y. Bao, H. Wang, F. Du, J. Tian, Q. Li, T. Wang and R. Bai, *J. Mater. Chem*., 2012, **22**, 3555.
98. J. He, M. Zha, J. Cui, M. Zeller, A. D. Hunter, S.-M. Yiu, S.-T. Lee and Z. Xu, *J. Am. Chem. Soc*., 2013, **135**, 7807.
99. A. L. Garner and K. Koide, *Chem. Commun*., 2009, **1**, 83.
100. H. Kim, S. Lee, J. Lee and J. Tae, *Org. Lett*., 2010, **12**, 5342.
101. D. Montagner, S. Q. Yap and W. H. Ang, *Angew. Chem. Int. Ed*., 2013, **52**, 11785.
102. C. Shen, B. D. W. Harris, L. J. Dawson, K. A. Charles, T. W. Hambley and E. J. New, *Chem. Commun*., 2015, **51**, 6312.
103. L. P. Bédard, K. H. Esbensen and S. J. Barnes, *Anal. Chem*., 2016, **88**, 3504.
104. M. Rodrigues, F. Cappa, M. Schreiner, P. Ferloni, M. Radtke, U. Reinholz, B. Woytek and M. Alram, *J. Anal. At. Spectrom*., 2011, **26**, 984.
105. L. Muchova, E. Bakker and P. Rem, *Water, Air, Soil Pollut Focus*., 2009, **9**, 107.
106. I. Birloaga, V. Coman, B. Kopacek and F. Vegliò, *Waste Manag*., 2014, **34**, 2581.
107. C. Bendall, D. Wigg-Wolf, Y. Lahaye, H.-M. von Kaenel and G. Brey, *Archaeometry*, 2009, **51**, 598.
108. M. Martinón-Torres and M. A. Uribe-Villegas, *J. Archaeol. Sci*., 2015, **63**, 136.
109. L. Dussubieux, M. Golitko and B. Gratuze, eds. Recent

Advances in Laser Ablation ICP-MS for Archaeology, Springer, Berlin, Heidelberg, 2016.

110. K. Avarmaa, H. O. Brien, H. Johto and P. Taskinen, *J. Sustain. Metall.*, 2015, **1**, 216.
111. S. Gilbert, L. Danyushevsky, P. Robinson, C. Wohlgemuth-Ueberwasser, N. Pearson, B. Savard, M. Norman and J. Hanley, *Geostand. Geoanalytical Res*., 2013, **37**, 51.
112. C. Gauert, M. Schannor, L. Hecht, M. Radtke and U. Reinholz, *Geostand. Geoanalytical Res*., 2016, **40**, 267.
113. M. Zelenski, V. S. Kamenetsky, J. A. Mavrogenes, L. V. Danyushevsky, D. Matveev and A. A. Gurenko, *Lithos*, 2017, **290-291**, 172.
114. J. H. Crocket, R. R. Keays and S. Hsieh, *J. Radioanal Chem*., 1968, **1**, 485.
115. M. Ebihara, S. Sekimoto, N. Shirai, Y. Hamajima, M. Yamamoto, K. Kumagai, Y. Oura, T. R. Ireland, F. Kitajima, K. Nagao, T. Nakamura, H. Naraoka, T. Noguchi, R. Okazaki, A. Tsuchiyama, A. Uesugi, H. Yurimoto, M. E. Zolensky, M. Abe, A. Fujimura, T. Mukai and Y. Yada, *Science*, 2011, **333**, 1119.
116. M. V. Frontasyeva, *Phys. Part. Nucl*., 2011, **42**, 332.
117. S. Sekimoto, N. Shirai and M. Ebihara, *J. Radioanal. Nucl. Chem*., 2016, **307**, 1757.
118. M. F. Guerra and T. Calligaro, *J. Archaeol. Sci*., 2004, **31**, 1199.
119. K. K. Swain, N. Ajith, R. Acharya, R. Verma and A. V. R. Reddy, *J. Radioanal. Nucl. Chem*., 2012, **294**, 319.
120. V. Zaichick and S. Zaichick, *J. Radioanal. Nucl. Chem*., 2009, **281**, 47.
121. S. Zaichick and V. Zaichick, *Biol. Trace Elem. Res*., 2010, **137**, 1.
122. S. Zaichick and V. Zaichick, *Appl. Radiat. Isot*., 2011, **69**, 827.
123. J. Tickner, R. Rajarao, B. Lovric and B. Ganly, *J. Sustain. Metall.*, 2016, **2**, 296.
124. T. X. Phuoc, P. Wang and D. McIntyre, *Fuel*, 2016, **163**, 129.
125. R. S. Harmon, R. R. Hark, C. S. Throckmorton, E. C. Rankey, M. A. Wise, A. M. Somers and L. M. Collins, *Geostand. Geoanalytical Res*., 2017, **41**, 563.
126. M. Ángel Aguirre, M. Hidalgo, A. Canals, J. A. Nóbrega and E. R. Pereira-Filho, *Talanta*, 2013, **117**, 419.
127. M. A. Gondal, Z. S. Seddigi, M. M. Nasrand B. Gondal, *J. Hazard. Mater*., 2010, **175**, 726.
128. G. Asimellis, N. Michos, I. Fasaki and M. Kompitsas, *Spectrochim. Acta, Part B: At. Spectrosc*., 2008, **63**, 1338.
129. S. Legnaioli, G. Lorenzetti, L. Pardini, V.Palleschi, D. M. DiazPace, F. Anabitarte Garcia, R. Grassi, F. Sorrentino, G. Carelli, M. Francesconi, F. Francesconiand R. Borgogni, *Spectrochim. Acta, Part B: At. Spectrosc*., 2012, **71-72**, 123.
130. Y. Lou, Q. Zhou and R. H. Li, *Adv. Mater. Res*., 2013, **706-708**, 752.
131. N. Ahmed, R. Ahmed and M. A. Baig, *Plasma Chem. Plasma Process*, 2018, **38**, 207.
132. M. Galiová, J. Kaiser, K. Novotný, J. Novotný, T. Vaculoviè, M. Liška, R. Malina, K. Stejskal, V. Adam and R. Kizek, *Appl. Phys. A: Mater. Sci. Process*, 2008, **93**, 917.
133. L. Pardini, A. El Hassan, M. Ferretti, A. Foresta, S. Legnaioli, G. Lorenzetti, E. Nebbia, F. Catalli, M. A. Harith, D. Diaz Pace, F. Anabitarte Garcia, M. Scuottoand V. Palleschi, *Spectrochim. Acta, Part B: At. Spectrosc*., 2012, **74-75**, 156.
134. H. E. Ahmed, Y. Liu, B. Bousquet, M. Baudelet and M. Richardson, *J. Text. Appar. Technol. Manag*., 2013, **8**, 1.
135. M. F. Guerra, *Radiat. Phys. Chem*., 2014, **95**, 356.
136. T. G. Weiszburg, K. Gherdán, K. Ratter, N. Zajzon, Z. Bendõ, G. Radnóczi, Á. Takács, T. Váczi, G. Varga and G. Szakmány, *Anal. Chem*., 2017, **89**, 10753.
137. K. Righter, L. R. Danielson, K. M. Pando, J. Williams, M. Humayun, R. L. Hervig and T. G. Sharp, *Meteorit. Planet. Sci*., 2015, **50**, 604.
138. F. Reith, C. M. Zammit, S. S. Shar, B. Etschmann, R. Bottrill, G. Southam, C. Ta, M. Kilburn, T. Oberthür, A. S. Ball and J. Brugge, *Nat. Geosci*., 2016, **9**, 294.
139. S. Sen Gupta, A. Baksi, P. Roy, D. Deb and T. Pradeep, *ACS Sustain. Chem. Eng*., 2017, **5**, 8310.
140. Q. Simon, D. Barreca, D. Bekermann, A. Gasparotto, C. Maccato, E. Comini, V. Gombac, P. Fornasiero, O. I. Lebedev, S. Turner, A. Devi, R. A. Fischer and G. V. Tendeloo, *Int. J. Hydrogen Energy*, 2011, **36**, 15527.
141. M. Banerjee, N. B. Srinivasan, H. Zhu, S. J. Kim, K. Xu, M. Winter, H.-W. Becker, D. Rogalla, T. de los Arcos, D. Bekermann, D. Barreca, R. A. Fischer and A. Devi, *Cryst. Growth Des*., 2012, **12**, 5079.
142. A. B. Djurišiæ, Y. H. Leung, A. M. Ng, X. Y. Xu, P. K. Lee, N. Degas and R. S. Wu, *Small*, 2015, **11**, 26.
143. K. Schütte, H. Meyer, C. Gemel, J. Barthel, R. A. Fischer and C. Janiak, *Nanoscale*, 2014, **6**, 3116.
144. E. Sutter, K. Jungjohann, S. Bliznakov, A. Courty, E. Maisonhaute, S. Tenney and P. Sutter, *Nat. Commun*., 2014, **5**, 1.
145. Y. Meng, F. Su and Y. Chen, *Sci. Rep*., 2016, **6**, 1.
146. I. L. Volkov, A. Smirnova, A. A. Makarova, Z. Reveguk, R. R. Ramazanov, D. Y. Usachov, V. K. Adamchuk and A. I. Kononov, *J. Phys. Chem. B*, 2017, **121**, 2400.